July 2025
Volume 54, Number 3



# AppliedRadiology®

The Journal of Practical Medical Imaging and Management

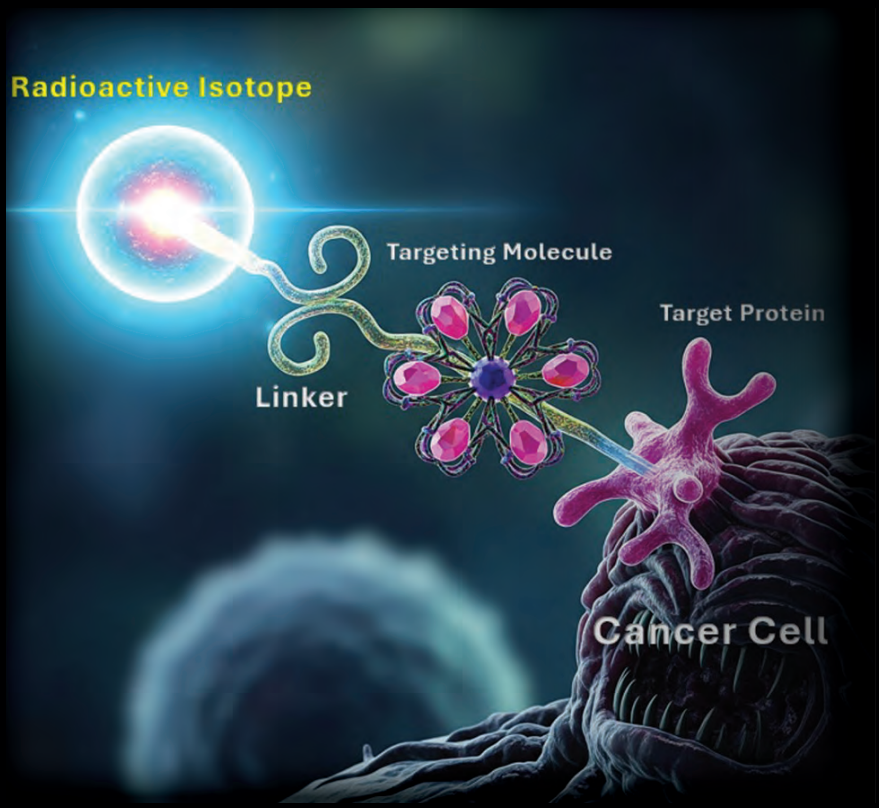


See It, Treat It: How Theranostics is Reshaping Cancer Care and Nuclear Medicine

You've Heard About CMS Dose-compliance in Radiology. What Does it Mean for You?

Post-Traumatic "Floating Fat" in the Extensor Tendon Sheaths of Wrist

Diagnostic Accuracy of Cerebroplacental Ratio in Anticipating Adverse Perinatal Outcome

Ankle Impingement Syndromes: What the Radiologist Needs to Know



www.appliedradiology.com

# AppliedRadiology®

The Journal of Practical Medical Imaging and Management

Anderson Publishing, Ltd
180 Glenside Avenue,
Scotch Plains, NJ 07076
Tel: 908-301-1995
Fax: 908-301-1997
info@appliedradiology.com




## Editorial Advisory Board

# AppliedRadiology®

The Journal of Practical Medical Imaging and Management

July 2025 Vol 54 No 3







Applied Radiology (ISSN 0160-9963) is published 6 times per year by Anderson Publishing, Ltd., with offices located at 180 Glenside Avenue, Scotch Plains, NJ 07076. Visit appliedradiology.com/subscribe to start your digital subscription. Any subscription queries should be emailed to appliedradiology@omeda.com.

# With Gratitude, Again

Erin Simon Schwartz, MD, FACR, FASPNR

**Dr Schwartz** is the editor-in-chief of *Applied Radiology*. She is the chief of the Division of Neuroradiology and holds the Robert A Zimmerman Chair in Pediatric Neuroradiology in the Department of Radiology at The Children's Hospital of Philadelphia. She is also professor of radiology, Perelman School of Medicine, University of Pennsylvania. She can be reached at erin@appliedradiology.com.

It is with quite mixed emotions that I come to you for the last time as Editor-in-Chief of *Applied Radiology*.

Serving in this position has been one of the highlights of my career. It has allowed me to step out of my uber-focused area of pediatric neuroradiology, engage with and learn so much from colleagues across all of Radiology's broad disciplines, as well as thought leaders in health care management, wellness, and sustainability. Meeting so many of our readers at our booth at RSNA each year has brought me special joy, especially hearing their wonderful comments about how what they have learned from *Applied Radiology* has influenced their practice and improved the care of their patients.

Of course, none of this would be possible without Kieran Anderson, our fearless leader, to whom I owe my deepest gratitude.

As Vice President and Group Publisher for Anderson Publishing, Kieran, along with the entire Anderson family, welcomed me as one of their own, and entrusted me with the leadership of their flagship journal for the past 6 years. I also owe my thanks to Joe Jalkiewicz, Sharon Breske, and Claudia Stahl, who have been outstanding editorial partners. Barbara Shopiro, Judy Murray, Carolyn Wellington, and Meaghan Honeck, too many thanks to you all for your support and for sharing your expertise. And, finally, to my husband, who has supported me through it all for over 20 years together, thank you so very much.

This has been a tremendous honor and I will miss my *Applied Radiology* family terribly.

But I have long been a believer in term limits and the importance of succession planning. To that end, I leave, secure in the knowledge that you are all in excellent hands.

I am thrilled to announce the new *Applied Radiology* Editor-in-Chief is Nina S. Vincoff, MD.

Many of our regular readers will recognize Dr. Vincoff's name from her active role in the Breast Imaging section on our editorial advisory board and the numerous review articles she has published with us.

Dr. Vincoff is the Breast Imaging Division Chief at Northwell Health, where she is also Medical Director at the Katz Institute for Women's Health and associate professor at the Donald and Barbara Zucker School of Medicine at Hofstra/Northwell in New York. A committed patient advocate, Dr. Vincoff is the Vice Chair of the American College of Radiology Patient and Family Centered Care Commission.

I wish Nina the greatest success; she brings tremendous energy and enthusiasm to the position, and I look forward to watching her take *Applied Radiology* to new heights. In joining the group of esteemed as Editors Emeriti, I do hope to stay engaged, including with the outstanding *Applied Radiology*/Bracco Leaders on the Horizon Program, to foster the next generation of radiology experts and leaders, as those who came before me so generously gave of their time and expertise for me.

To that end, in my final issue we are sharing the first-place winners in the review paper and original research categories from last year's Leaders on the Horizon Program as testament to their work and as a reminder to all residents to submit their papers for this year's program before September 1 at https://appliedradiology.com/leaders. I look forward to reading your submissions.

Stay well.

Published: July 1, 2025. https://doi.org/10.37549/AR-D-2025-0092

# See It, Treat It: How Theranostics Is Reshaping Cancer Care and Nuclear Medicine

Alireza Amindarolzarbi, MD; Elliot Siegel, MD


## Abstract

Theranostics, the integration of diagnostic imaging and targeted therapy, is revolutionizing the field of nuclear medicine. This review explores its origins, clinical applications, future directions, and its potential as a transformative career path for radiologists and nuclear medicine physicians. Beginning with the pioneering use of radioactive iodine, theranostics has evolved into a precision medicine tool with landmark examples like lutetium Lu 177 dotatate (Lutathera) for neuroendocrine tumors and lutetium Lu 177 vipivotide tetraxetan (Pluvicto) for prostate cancer. The concept of 'theranostic twins'—radioactive drugs sharing a molecular target but used for imaging or therapy—has allowed for unparalleled treatment specificity. We discuss mechanisms of action, clinical trials such as NETTER-1 and PSMAfore, and the emerging role of dosimetry in individualizing treatment. Barriers including regulatory complexity, reimbursement, and infrastructure requirements are analyzed, along with future advances in α emitters, novel ligands, and applications beyond oncology. With growing interest from trainees, evolving training pathways, and increasing institutional investment, theranostics represents a powerful new frontier in personalized medicine.


**Keywords:** theranostics, radiology, nuclear medicine, molecular imaging, radiopharmaceutical therapy, lutetium-177, Pluvicto, targeted therapy, PET/CT, dosimetry

## Introduction

The 1966 science fiction film "Fantastic Voyage" depicted a miniaturized medical team navigating the bloodstream to diagnose and treat a brain lesion. Now, nearly 60 years later, the emerging medical specialty of "theranostics" is realizing this vision in a novel and precise form. Theranostics used diagnostic imaging and molecularly targeted radionuclides thousands of times smaller than the fictional Proteus submarine to diagnose and treat specific cancers. The rapid growth of theranostics in the United States is driving a transformative shift in the field of nuclear medicine.

As theranostics expands, a foundational understanding of theranostic principles and applications is becoming essential for today's radiologists and nuclear medicine physicians. The term "theranostics," a portmanteau of "therapy" and "diagnostics" originally coined in 1998, also represents a new career pathway for trainees who are interested in a specialty that combines direct patient care with diagnostic and interventional molecular imaging.

**Affiliation:** Department of Diagnostic Radiology and Nuclear Medicine, University of Maryland, Baltimore, Maryland.
**Disclosures:** The authors have no conflicts of interest to disclose. None of the authors received outside funding for the production of this original manuscript and no part of this article has been previously published elsewhere.
**Declaration on the Use of AI:** The authors of this manuscript declare that in the writing process of this work, no generative artificial intelligence (AI) or AI-assisted technologies were used to generate content, ideas, or theories. We utilized AI solely for the purpose of enhancing readability and refining language. This use was under strict human oversight and control. After the application of AI technologies, the authors carefully reviewed and edited the manuscript to ensure its accuracy and coherence.

Published: July 1, 2025. https://doi.org/10.37549/AR-D-0084

Drs. Saul Hertz and Arthur Roberts at Massachusetts General administered the first theranostic treatment using iodine-131 ($^{131}$I) to both image and treat hyperthyroidism on March 31, 1941 (now recognized as Theranostics Day), and subsequently, the first thyroid cancer patient the following year. The use of iodine-123 ($^{123}$I) for imaging and $^{131}$I for therapy marked the first theranostic pair. The "renaissance" in theranostics has been driven by a combination of progress in understanding cancer biology, the identification of specific molecular targets on cancer cells, and advances in radiochemistry and targeting ligands such as peptides and small molecules. Recent breakthroughs in molecular targeting and radiochemistry have led to the development of highly effective radiopharmaceutical therapies, notably lutetium Lu 177 dotatate (Lutathera) approved by the United States Food and Drug Administration (FDA) for neuroendocrine tumors in 2018, and lutetium Lu 177 vipivotide tetraxetan (Pluvicto), approved for prostate cancer in 2022.

The phrase "theranostic pair" refers to 2 radioactive drugs that target the same molecular structure—such as a receptor, transporter, or antigen—that may be expressed on cancer cells, within the tumor microenvironment, or on supporting stromal or immune cells, but incorporate different radionuclides for imaging versus therapy. One isotope is chosen for its imaging properties, and the other is selected for its therapeutic properties (delivering a dose of radiation to kill the targeted cells) (Figure 1).

The primary mechanism by which a theranostic molecule attaches to a cancer cell involves a highly selective binding interaction between a targeting ligand on the theranostic molecule and a corresponding receptor or antigen that is either overexpressed or uniquely present on the cancer cell membrane. Common targeting ligands used in theranostic molecules include antibodies, peptides, small molecules, and aptamers (Table 1).

**Figure 1.** Conceptual drawing of a radiopharmaceutical made up of a radioactive isotope, linker, and targeting molecule complex which attaches to a target protein on a cancer cell.

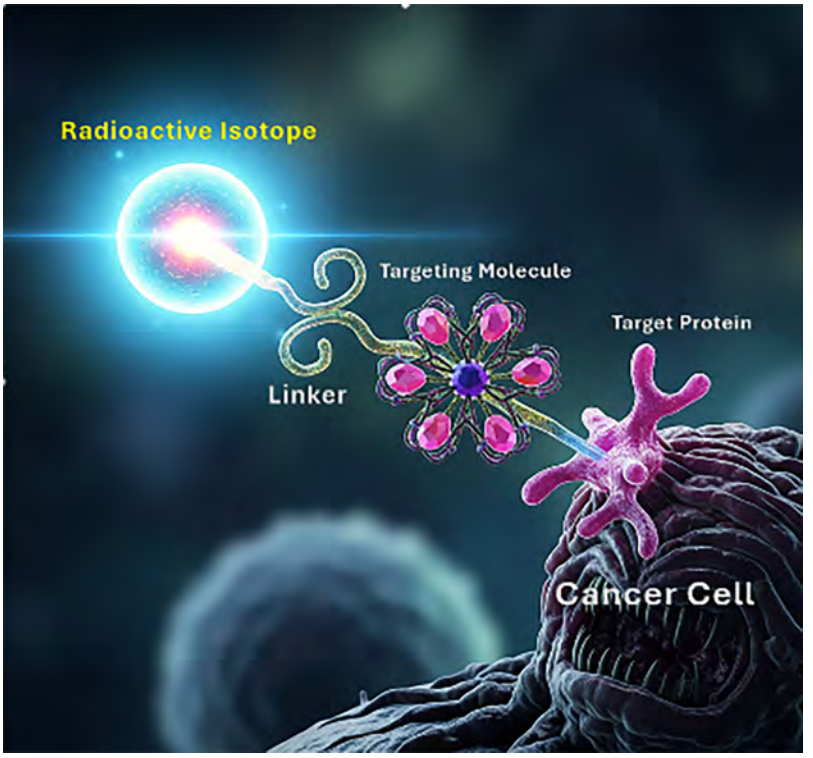


A PET/CT scan is performed using a diagnostic twin such as $^{68}$Ga-DOTATATE (Gallium-68 DOTA-[Tyr$^3$]-octreotate) (68-minute half-life) or $^{64}$Cu-DOTATATE (Copper-64 DOTA-[Tyr$^3$]-octreotate) (12.7-hour half-life) to image somatostatin receptors, which are overexpressed in several neuroendocrine tumor types. If the scan shows sufficient uptake of the diagnostic agent, it suggests that the patient is likely to benefit from the therapeutic twin, which in the case of neuroendocrine tumors is lutetium Lu 177 dotatate. Using the same targeting molecule, it travels to and binds to the same cancer cells identified in the scan, then emits a β particle (a high-energy electron) that disrupts the tumor DNA while minimizing radiation exposure to surrounding healthy tissues. Studies such as NETTER-1 provide compelling evidence indicating that patients experience prolonged survival without disease progression and report enhanced quality of life in patients with advanced, progressive, and well-differentiated somatostatin receptor-positive midgut neuroendocrine tumors.[1] Progression-free survival (PFS) in patients treated with lutetium Lu 177 dotatate plus Octreotide LAR (long-acting release) improved to 28-29 months compared with 8.4 months with high-dose octreotide LAR alone. The NETTER-2 trial was the first to evaluate lutetium Lu 177 dotatate as a first-line treatment and included patients with grade 2 and grade 3 advanced gastroenteropancreatic

**Table 1. Common Targeting Ligands Used in Theranostic Molecules**

| TARGETING LIGAND TYPE | DESCRIPTION |
|---|---|
| Antibodies | Proteins that naturally bind with high specificity to certain antigens. Monoclonal antibodies can be engineered to recognize antigens that are abundant on cancer cells. |
| Peptides | Short chains of amino acids that can be designed to bind to specific receptors on cancer cells. |
| Small molecules | Smaller chemical compounds that can be synthesized to target and bind to specific molecules or pathways involved in cancer cell growth and survival. |
| Aptamers | Nucleic acid (DNA or RNA) molecules that can fold into specific 3D structures to bind to target molecules with high affinity and specificity. |

neuroendocrine tumors, again comparing long-acting octreotide alone with combination therapy with lutetium Lu 177 dotatate. Median PFS was extended to 22.8 months compared with 8.5 months for patients receiving combination therapy with a higher objective response rate of 43% versus 9% for the combination therapy, with a small percentage of patients in the lutetium Lu 177 dotatate arm achieving a complete response. Patients receiving lutetium Lu 177 dotatate typically undergo 4 cycles of therapy that are 8 weeks apart.

In the case of prostate cancer, the diagnostic twins currently FDA approved are $^{68}$Ga-PSMA-11 (gallium-68-labeled prostate-specific membrane antigen-11), $^{18}$F-DCFPyL (fluorine-18-labeled 2-(3-{1-carboxy-5-[(6-[$^{18}$F]fluoro-pyridine-3-carbonyl)-amino]-pentyl}-ureido)-pentanedioic acid), and $^{18}$F-rhPSMA-7.3 (fluorine-18-labeled radiohybrid prostate-specific membrane antigen ligand 7.3). These bind to prostate-specific membrane antigen (PSMA), which is commonly overexpressed in patients with prostate cancer. This enables direct visualization of the PSMA distribution throughout the body. Lutetium Lu 177 vipivotide tetraxetan serves as the therapeutic twin by first binding to the PSMA receptor on the surface of a prostate cancer cell and causing endocytosis of the PSMA receptor-$^{177}$Lu-vipivotide tetraxetan complex. Once inside, β particles are released, damaging the cancer cell's DNA and ultimately leading to cell death (Figure 2).

Lutetium Lu 177 vipivotide tetraxetan is currently FDA approved for PSMA-positive metastatic castration-resistant prostate cancer patients who have been treated with an androgen receptor pathway inhibitor and either

1. have previously received taxane-based chemotherapy or
2. as of April 2025 are eligible for treatment prior to receiving taxane-based chemotherapy.

This latest expanded indication for lutetium Lu 177 vipivotide tetraxetan [1] was based on the PSMAfore trial. The trial demonstrated that in patients who had progressed after an androgen receptor pathway inhibitor and had not yet received chemotherapy, lutetium Lu 177 vipivotide tetraxetan achieved a 57% reduced risk of radiographic progression or death and more than doubled median radiographic PFS from 5.6 months to 12.0 months compared with patients switched to another androgen receptor pathway inhibitor.[2] Additionally, patients treated with lutetium Lu 177 vipivotide tetraxetan had a 51% versus 15% objective response rate (tumor reduction in size demonstrated with imaging) and 58% versus 20% significant decline in PSA levels. Patients receiving lutetium Lu 177 vipivotide tetraxetan typically undergo up to 6 treatment cycles, each spaced 6 weeks apart.

## Dosimetry for Theranostics

Unlike chemotherapy, which delivers cytotoxic agents systemically with limited ability to measure in vivo distribution, post-therapy "dosimetry" using SPECT/CT allows precise assessment of how much of the injected dose is delivered to tumor cells as well as organs at risk, such as the kidneys, liver, and bone marrow. Dosimetry data for lutetium Lu 177 dotatate and lutetium Lu 177 vipivotide tetraxetan are obtained through multiple SPECT/CT studies post-therapy. Given the 6.7-day half-life of $^{177}$Lu, these studies can track the clearance of the injected radiopharmaceutical from tumors and organs at risk at early (a few hours after injection) and multiple intermediate time points, days after the initial therapy. Given the current "one-dose-fits-all" FDA approval, dosimetry can inform theranostic providers about potential toxicities for organs at risk (eg, renal, liver, and bone marrow), educate patients about their treatment, and provide quality assurance. In the future, when doses and timing of delivery of doses will be customized to individual patients, dosimetry will play a major role in optimizing delivery of the correct dose to tumors while keeping toxicity at acceptable levels. This will enable the optimization of dosing and time tailored to individual patients, iteratively balancing tumor control and organ toxicity in a way that is not possible with other cancer treatments.

**Figure 2.** Mechanism of action for lutetium Lu 177 vipivotide tetraxetan (Pluvicto). The radioligand targets PSMA receptors on prostate cancer cells, is internalized through endocytosis, and releases β particles intracellularly, inducing DNA damage and cell death. Each prostate cancer cell can ingest (internalize) multiple radioligands.

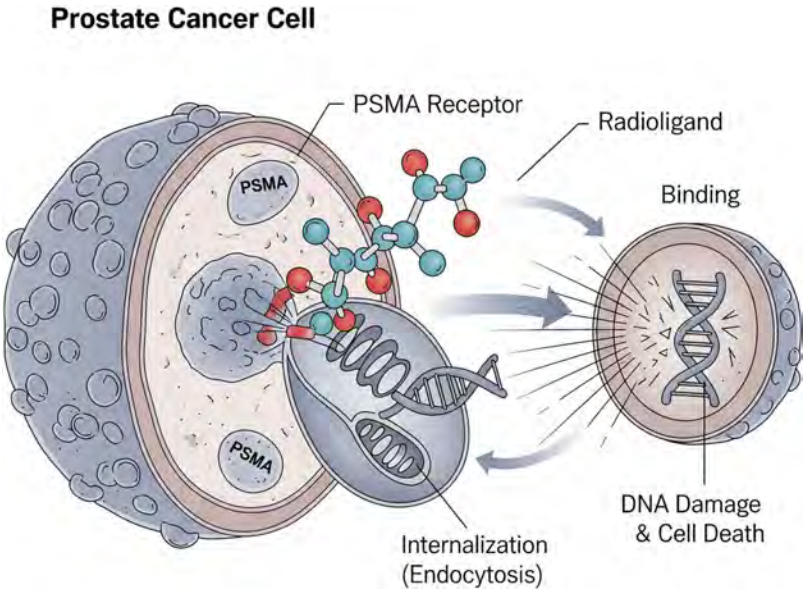


**Figure 3.** Projected growth of the global theranostics market. According to Fortune Business Insights, the market is expected to expand from $4.75 billion in 2025 to $27.76 billion by 2032, representing a compound annual growth rate (CAGR) of 28.7%.

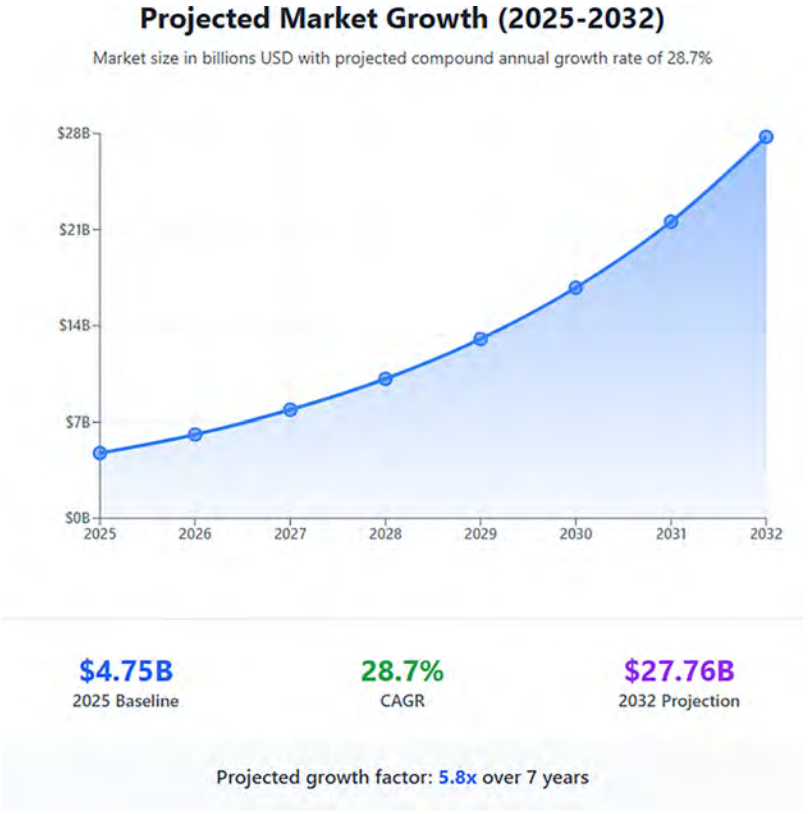


## What's Next?

The field of theranostics is advancing at a breathtaking rate, with nanoparticle therapy emerging as a versatile platform for delivering therapeutic agents. The global theranostics market size is also expanding exponentially, driven by significant investments in new radiopharmaceuticals (Figure 3).

While β emitters such as $^{177}$Lu are now well established, α emitters such as actinium-225 are gaining significant traction. α particles are made of a helium nucleus, which is made up of 2 neutrons and 2 protons. α particles have a molecular mass of more than 7000 times that of a β particle and are much more disruptive to both DNA strands of a cancer cell and have a shorter range (50-100 microns). The higher linear energy transfer of α particles allows them to behave more like a scalpel than β particles, which are more akin to a shotgun. By damaging DNA directly and rapidly, their efficacy is unaffected by cell cycle stage, tumor hypoxia, or resistive tumor cell adaptations, as commonly seen with chemotherapy and other types of therapy. Innovative targeting ligands are being engineered to target a much broader range of cancer-specific markers. The 5 cancer types that seem to be on the relatively short-term horizon for theranostic therapy include pancreatic, breast, lung, melanoma, multiple myeloma, and leukemia (Table 2).

The field of theranostics is rapidly extending its applications beyond oncology. Researchers are exploring potential applications in cardiovascular medicine, where PET agents can identify molecular markers of inflammation and plaque instability, laying the groundwork for a future theranostic approach.[3] Theranostic agents are being designed to visualize and

**Table 2. The Five Cancer Types on the Near Horizon for Theranostic Therapy and Their Targets**

| CANCER TYPE | TARGET | DETAILS |
|---|---|---|
| Pancreatic | CLDN4, fibroblast activation protein | Claudins are tight junction proteins that are overexpressed in pancreatic cancer; fibroblasts are abundant in pancreatic and many other types of cancer |
| Breast | HER2, Trop-2 | Well established as targets for antibody-drug conjugates |
| Non-small cell and small cell lung cancer | DLL3, EGFR | DLL3 is an emerging target for small cell lung cancer and other high-grade neuroendocrine tumors; EGFR is a cornerstone target in NSCLC |
| Melanoma | Melanocortin 1 receptor | MC1R, which plays a role in pigmentation, is overexpressed in melanoma cells |
| Multiple myeloma and leukemia | C-X-C chemokine receptor 4 | CXCR4 is involved in how hematopoietic cancer cells traffic to and anchor in the bone marrow |

target β-amyloid plaques and tau tangles in Alzheimer's disease.[4] Other potential applications under development include the targeted delivery of antibiotics or antiviral medications to sites of infection and the diagnosis and treatment of autoimmune diseases.

## Challenges to the Field of Theranostics

The FDA requires a particularly rigorous and lengthy approval process for combination products (eg, diagnostic and therapeutic twins), which often require separate or coordinated submissions and reviews by multiple FDA centers. Designing clinical trials in humans to effectively prove both safety and efficacy is a complex and highly expensive process. Securing consistent and adequate reimbursement from the Centers for Medicare & Medicaid Services (CMS) and private payors is another key but arduous process, even after FDA approval. While CMS has recently moved to "unbundle" reimbursement for higher-cost diagnostic radiopharmaceuticals, the complexities of billing and coding for both diagnostic and therapeutic components of theranostics remain a significant challenge for health care providers. Supply chain challenges were evident in recent months, including shortages in the global supply of $^{177}$Lu and $^{68}$Ga, and ramping up domestic production requires major investments in infrastructure such as cyclotrons and processing facilities.

Additionally, the administration of radiopharmaceuticals requires specialized infrastructure, including dedicated shielded infusion rooms, hot labs, PET/CT, and SPECT/CT. The specialized training required to operate the equipment poses recurrent staffing costs from nuclear technicians, specialty-trained radiologists, and nuclear medicine physicians. The sub-specialized knowledge of how to administer these radiopharmaceuticals to patients safely, interpretation of complex multi-modality imaging studies, and the nuanced subtleties and complexities of radiation dosimetry are beyond the experience and training of the vast majority of current inpatient and outpatient diagnostic radiology, radiation oncology, and nuclear medicine practices.

An increasing number of medical students and residents are expressing an interest in a career in this exciting and pioneering field. Theranostics uniquely combines diagnostic imaging with direct patient care guided by a particularly individualized treatment paradigm. Entrepreneurial skills are also necessary to build and grow a thriving practice, as even experienced oncologists and urologists are often unaware of theranostics. As we are seeing at our own institution, an increasing number of applicants are being drawn to nuclear medicine and radiology with the intention of combining their intersecting interests in diagnostic imaging, oncology, and patient care to establish a theranostics practice.

Theranostics training is being incorporated into nuclear medicine residency programs as a foundational part of future practice, as well as part of the American Board of Radiology (ABR) 16-month pathway within a diagnostic radiology residency that can lead to a sub-specialty certificate in nuclear radiology. They are also being incorporated into radiation oncology training programs. Dedicated formal fellowship programs are currently being offered at several academic medical centers, including the University of Washington, Massachusetts General Hospital, Duke University, the University of Iowa, and Wake Forest University. These typically offer a special focus on oncologic nuclear medicine and radiopharmaceutical therapies.

In the future, as theranostics becomes increasingly widespread for a growing diversity of cancers, one could imagine an additional track in diagnostic radiology training programs in addition to the internship plus 4-year diagnostic

radiology and 6-year interventional radiology (that includes the internship year) pathways that would focus on "interventional targeted molecular therapy" with added experience in direct patient care, similar to that offered in the interventional radiology with an emphasis on ownership of the patient's oncologic journey through long-term follow-up and individualized treatment regimens.

## Conclusion

The rapidly developing field of theranostics represents a paradigm shift in precision medicine, evolving from a conceptual "fantastic voyage" to a clinical reality that will reshape the landscape of diagnostic radiology, nuclear medicine, and oncology.

While significant challenges in regulatory approval, reimbursement, and infrastructure remain, the rapid pace of innovation, from novel targeting ligands and α emitters to expanding applications in cardiovascular and neurological disease, promises an even more impactful future. For radiology and nuclear medicine residents, this dynamic field presents an exciting and rewarding career pathway, merging the intellectual rigor of diagnostic interpretation with the profound fulfillment of direct, life-altering patient therapy. Theranostics is poised to become a new cornerstone of 21st century medicine, offering renewed hope for patients and a new frontier for the next generation of physicians.

## References

1) Strosberg J, El-Haddad G, Wolin E, et al. Phase 3 trial of 177Lu-Dotatate for midgut neuroendocrine tumors. *N Engl J Med*. 2017;376(2):125-135. doi:10.1056/NEJMoa1607427

2) Morris MJ, Castellano D, Herrmann K, et al. 177Lu-PSMA-617 versus a change of androgen receptor pathway inhibitor therapy for taxane-naive patients with progressive metastatic castration-resistant prostate cancer (PSMAfore): a phase 3, randomised, controlled trial. *Lancet*. 2024;404(10459):1227-1239. doi:10.1016/S0140-6736(24)01653-2

3) Tarkin JM, Joshi FR, Evans NR, et al. Detection of atherosclerotic inflammation by $^{68}$Ga-DOTATATE PET compared to [$^{18}$F]FDG PET imaging. *J Am Coll Cardiol*. 2017;69(14):1774-1791. doi:10.1016/j.jacc.2017.01.060

4) Mout R, Ray M, Yesilbag Tonga G, et al. Theranostic nanosystems for neurodegenerative diseases. *Adv Sci (Weinh)*. 2021;8(17):e2100877. doi:10.1002/advs.202100877

# What Does CMS Dose Compliance in Radiology Mean for You?

Ari Goldberg, MD, PhD

Ari Goldberg is Director of Cardiothoracic and Abdominal Imaging at Loyola University Health System, Highland Park, IL

## Background

### First, the Short Answer

The Centers for Medicare & Medicaid Services (CMS) has slated voluntary public reporting of metrics related to radiation dose and image quality in calendar years 2025 and 2026, with mandatory reporting beginning in 2027. While the financial incentives or penalties tied to performance remain to be defined, institutions should be preparing for the inclusion of such compliance and reporting in broader CMS quality and payment programs.[1] These temporal horizons are clearly moving toward us, so any radiology practice would be wise to proactively consider the installation or refinement of appropriate software and workflow to be compliant.

### Wait, How Did We Get Here? (The Longer Answer)

Computed tomography (CT) radiation doses, even when administered for identical clinical indications, can vary dramatically across patients, institutions, and scanner models, a variability that has been historically driven more by practice preferences than by consistent evidence-based thresholds. Although the American College of Radiology's Dose Index Registry enables benchmarking of local dose performance against regional and national aggregates, it offers no mandatory dose limits or formal guidance on what constitutes an excessive dose.[2] Indeed, a phantom-based study of standard body CT protocols revealed dose exposures that differed significantly depending on the specific scanner used, indicating that even patients of similar size may receive widely disparate radiation levels for the same exam.[3]

While quantifying the effects of ionizing radiation from CT involves extrapolation and some uncertainty, the consensus continues to be that it carries a nontrivial risk of inducing malignancy, particularly when cumulative exposures are considered over a lifetime. The National Academies' BEIR VII Phase 2 report remains the authoritative source on low-level radiation risk, estimating increased cancer incidence in exposed populations based on epidemiologic and mechanistic data.[4] Given this risk profile, the absence of standardized dose thresholds against the backdrop of growing CT utilization presents patient-safety and public-health concerns.

In response, CMS contracted the University of California San Francisco in 2019 to develop a formal quality measure addressing radiation dose in diagnostic CT exams.[5] Recognizing that dose reduction efforts must preserve diagnostic value, the resulting measure incorporates image noise thresholds and combines three key elements: scanner-reported dose adjusted for patient size, a global noise metric, and classification of each study into one of 18 CT categories defined by body region and clinical indication. Thus, for each category, CMS specifies paired dose-and-noise thresholds and studies whose measured dose or noise fall outside these limits are defined as out of range.[5]

Published: July 1, 2025. https://doi.org/10.37549/AR-D-25-0088


The benchmarking data underpinning the measure were derived from a registry of 4.5 million adult CT exams, across 383 scanners representing 74 distinct models, in the UCSF International CT Dose Registry. Median and 75th-percentile dose levels varied by up to an order of magnitude within categories, validating the need for category-specific benchmarks and optimization.[6] Thresholds were then established based upon image-quality evaluation of 200 CT exams by 125 radiologists such that dose thresholds corresponded to at least 90% of radiologists judging image quality to be adequate, and noise thresholds were defined as the point at which 25% of radiologists rated the image quality as inadequate.[7]

Following multisite pilot testing, the National Quality Forum endorsed the measure for hospital and physician-level quality assessment, marking it as the first radiology measure to receive such recognition.[5]

### OK, So We Have a Radiation and Quality Measure. Now What?

Implementing the measure in a practical manner involves conversion to an electronic clinical quality measure (eCQM); it is this eCQM that will be reported to CMS. Because the eCQM framework was not designed to integrate DICOM Radiation Dose Structured Reports or raw image noise data directly, hospitals must translate radiology data into the standardized format required for eCQM submission. However, there is considerable confusion in the general radiology ecosystem, among practices and the marketplace, as to what is actually required in this process by CMS.

To begin with, satisfactory measure reporting can be achieved *either* through EHR-embedded eCQM modules (such as EPIC) or via third-party software that extracts, normalizes, and submits the data directly to CMS. There is no requirement by CMS to use any particular software vendor. In fact, a clarification to this effect was recently published by CMS on January 30, 2025. Indeed, the market already contains vendors who offer reporting via multiple methods. For example, ALARA and Imalogix both offer FHIR, HL7, and CSV outputs for EHR integration.

Furthermore, as clarified by CMS in the same January 30, 2025 release, no single vendor or proprietary platform is required—*any software meeting the measure's specifications may be used*, and

hospitals are not obligated to demonstrate vendor approval to CMS.[8] In fact, CMS does not—and has never—required that different software from different vendors even produces the exact same output.[9,10] Rather, CMS only requires a software solution that works within the "measure specifications," i.e., use of the 18 CT categories and use of size-adjusted dose.

While this last point may seem a bit counterintuitive, it is actually quite consistent with the nature of the measure. To understand how slight variations can arise, it is instructive to look at a specific component. For example, the size-adjusted radiation dose is calculated as

$$\text{Size} - \text{Adjusted Dose} = D_R \times \exp(-(d - d_k) \times \beta_k)$$

where $d$ is the patient's effective anatomic diameter—but there are many potential variations in diameter measurement techniques: Is the patient's diameter measured at one point (ie, the mid-point of the scan) or does it represent an aggregate value (ie, average or median across the scan)? Is diameter measured in the lateral and AP directions to calculate the effective diameter, or is the area of the patient used to compute the effective diameter? $d_k$ is the expected, or reference, diameter for the assigned CT category, derived from the registry's median exam diameters. However, its utilization is not formalized, and other registries and databases may yield small discrepancies in this variable.

Thus, subtle differences in dose calculations can exist across sites and software,[8] while still being acceptable to CMS.

## The Upshot

Individual practices should survey the landscape and see which solution works best for them, including providers such as Imalogix, ALARA, or others.

The reporting deadlines are approaching, and there are a few avenues of thought and action that should be common to all radiology departments at this time:

- **Validate data pipelines** to ensure accurate extraction and mapping of dose and noise metrics to whichever software solution is chosen.
- **Evaluate eCQM solutions** for seamless integration with existing EHR and/or PACS workflows.
- **Engage multidisciplinary stakeholders**—IT, quality, compliance, and clinical teams—to establish governance for data review and exception management.
- **Monitor performance continuously** to identify outliers and drive iterative optimization.

By embracing this standardized measurement framework, institutions can reduce unnecessary radiation exposure, uphold diagnostic quality, and align with CMS's evolving quality-reporting landscape, regardless of the specific software solution employed.

## References

1) Wells JR, Christianson O, Gress DA, et al. The new CMS measure of excessive radiation dose or inadequate image quality in CT: issues and ambiguities-perspectives from an AAPM-commissioned panel. *AJR Am J Roentgenol.* 2025;224(5):e2432458. doi:10.2214/AJR.24.32458

2) American College of Radiology. Dose index. Accessed June 17, 2025. https://www.acr.org/Clinical-Resources/Clinical-Tools-and-Reference/Registries/Dose-Index

3) Jaffe TA, Yoshizumi TT, Toncheva G, et al. Radiation dose for body CT protocols: variability of scanners at one institution. *American Journal of Roentgenology.* 2009;193(4):1141-1147. doi:10.2214/AJR.09.2330

4) Committee to Assess Health Risks from Exposure to Low Levels of Ionizing Radiation, National Research Council. *Health Risks from Exposure to Low Levels of Ionizing Radiation: BEIR VII Phase 2.* National Academies Press; 2006.

5) Smith-Bindman R, Kohli M. How to comply with CMS's CT radiation dose measure. Accessed June 27, 2004. https://www.auntminnie.com/clinical-news/ct/article/15678440/how-to-comply-with-cmss-ct-radiation-dose-measure

6) Smith-Bindman R, Yu S, Wang Y, et al. An image quality-informed framework for CT characterization. *Radiology.* 2022;302(2):380-389. doi:10.1148/radiol.2021210591

7) Smith-Bindman R, Wang Y, Stewart C, et al. Improving the safety of computed tomography through automated quality measurement: a radiologist reader study of radiation dose, image noise, and image quality. *Invest Radiol.* 2024;59(8):569-576. doi:10.1097/RLI.0000000000001062

8) Electronic Clinical Quality Improvement (ECQI) Resource Center. Excessive radiation dose or inadequate image quality for diagnostic Computed Tomography (CT) in adults (Facility IQR). Accessed June 17, 2025. https://ecqi.healthit.gov/ecqm/eh/2025/cms1074v2

9) National Quality Forum. Project measures. Accessed June 17, 2025. https://www.qualityforum.org/ProjectMeasures.aspx?projectID=86057&cycleNo=2&cycleYear=2021

10) Federal Register. Final rule. 2023;88(224):3624; 2023. Accessed June 17, 2025. https://www.federalregister.gov/d/2023-24293/p-3624

July 2025
As seen in *Applied Radiology*

# Best Practices for $^{68}$Ga-PSMA-11 PET Imaging: Dose Optimization From Real-World Insights

Telix
SPONSORED ARTICLE

# Best Practices for $^{68}$Ga-PSMA-11 PET Imaging: Dose Optimization From Real-World Insights

Colton L Cox[1], Guy Jones[2]

Prostate-specific membrane antigen (PSMA) positron emission tomography (PET) imaging using $^{68}$Ga-PSMA-11 is an integral tool for the detection and management of prostate cancer, particularly for patients with suspected metastasis who are candidates for initial staging, with suspected biochemical recurrence, and with metastatic castration-resistant prostate cancer who are candidates for PSMA-directed radioligand therapy.[1-4] The clinical efficacy and safety of dosing patients with 3 to 7 mCi, as per US prescribing information, is well established.[1,4,5] We present best practices for dosing based on foundational principles of nuclear medicine and extensive real-world experience from our high-volume site where we utilize a standard dose of 6 to 7 mCi as best practice.

In PET imaging, the final image quality is fundamentally tied to the number of detected coincidence events, which is influenced positively by higher radiotracer dose and longer scan times and negatively by larger patient body habitus and older PET scanner technology.[6-8] Higher injected doses result in greater positron emissions, leading to increased count statistics and, theoretically, improved image quality; however, this relationship is not linear and exhibits a peak at moderate dose levels.[7] Longer scan time may also improve image quality by increasing coincidence events; however, it often negatively impacts patient comfort and overall experience.[7] Conversely, larger body habitus often lead to greater photon attenuation and scatter, which can reduce image quality if not accounted for.[8] Additionally, older PET scanner technology may have impaired count-rate capabilities, producing images with high noise, and have a short axial field of view, limiting detection sensitivity and image resolution.[9-12] In a retrospective analysis of 856 patients with biochemically recurrent prostate cancer who underwent $^{68}$Ga-PSMA-11 PET, detection rates were 10% higher with the newer PET system (76%) compared to an older model (66%).[9] Notably, over 50% of PET scanners in the US were installed prior to 2014.[13,14]

For reasons discussed above, many physicians and sites have started to follow a best practice of dosing patients within the 6 to 7 mCi range, with over 1,000 patients having received a 6 to 7 mCi dose of $^{68}$Ga-PSMA-11 to date.[15] Our site experience further supports this best practice. We present a series of case images taken on a Siemens Biograph mCT-S (40) 3R PET/CT scanner (scanner introduced to the US market in 2009) from patients across a wide array of body habitus (body mass index [BMI] range, 25 to >40 kg/m$^2$) and several with micrometastatic disease. These real-world cases are intended to support clinicians with practical insights and rationale for establishing this best practice, which further augments the flexibility and optimal imaging allotted with $^{68}$Ga-PSMA-11 PET.

**Affiliations:** [1]University of Nevada, Reno School of Medicine, Reno, Nevada, US; [2]Oncology Nevada, Reno, Nevada, US
**Disclosures:** Medical writing support provided by Grace Wang (Telix Pharmaceuticals).

**Figure 1.** $^{68}$Ga-PSMA-11 PET/CT showing PSMA avid disease in pelvic lymph nodes. (A) Transversal fused PET/CT, (B) coronal fused PET/CT, and (C) CT.

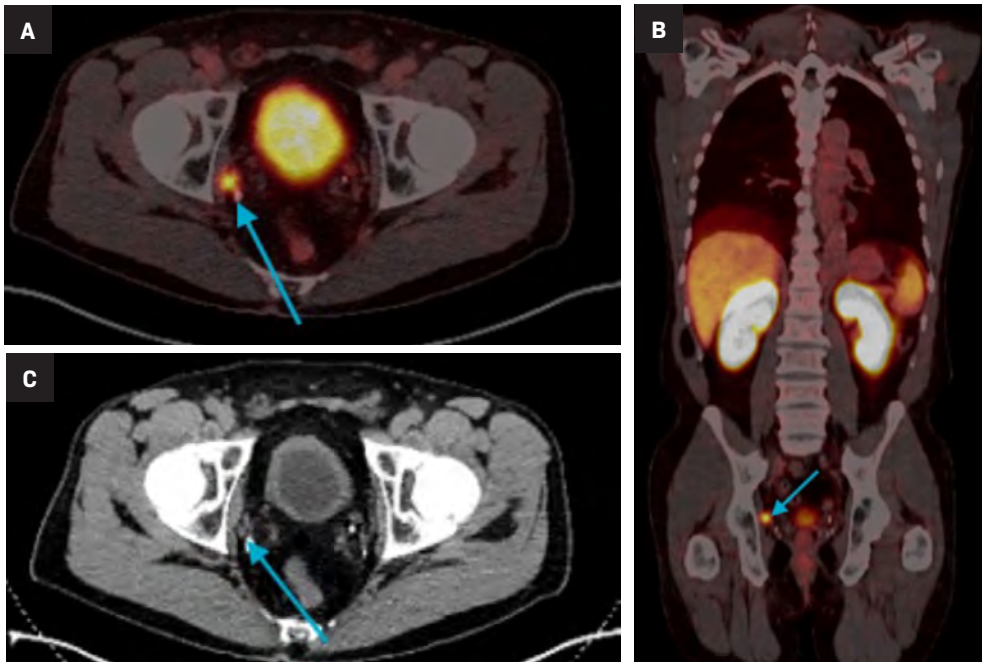


## Patient #1

A 67-year-old male with a BMI >25 kg/m$^2$ underwent robot-assisted laparoscopic prostatectomy (RALP) for clinically localized prostate adenocarcinoma. Final pathology revealed pT3aN0M0 disease with a Gleason score of 4+3=7 and a preoperative prostate-specific antigen (PSA) level of 6.85 ng/mL. Postoperatively, the patient exhibited a persistently detectable PSA level of 0.25 ng/mL. A year later, $^{68}$Ga-PSMA-11 PET/CT (7.0 mCi; 54-minute uptake; 2 minutes/bed for 10 beds; total scan time 20 minutes) demonstrated radiotracer uptake in pelvic lymph nodes, consistent with regional metastatic involvement (Figure 1). The patient is scheduled to undergo salvage radiation therapy in conjunction with androgen deprivation therapy (ADT), including relugolix and apalutamide.

**Figure 2.** $^{68}$Ga-PSMA-11 PET/CT showing PSMA avid disease in prostate. (A) Transversal fused PET/CT and (B) CT.

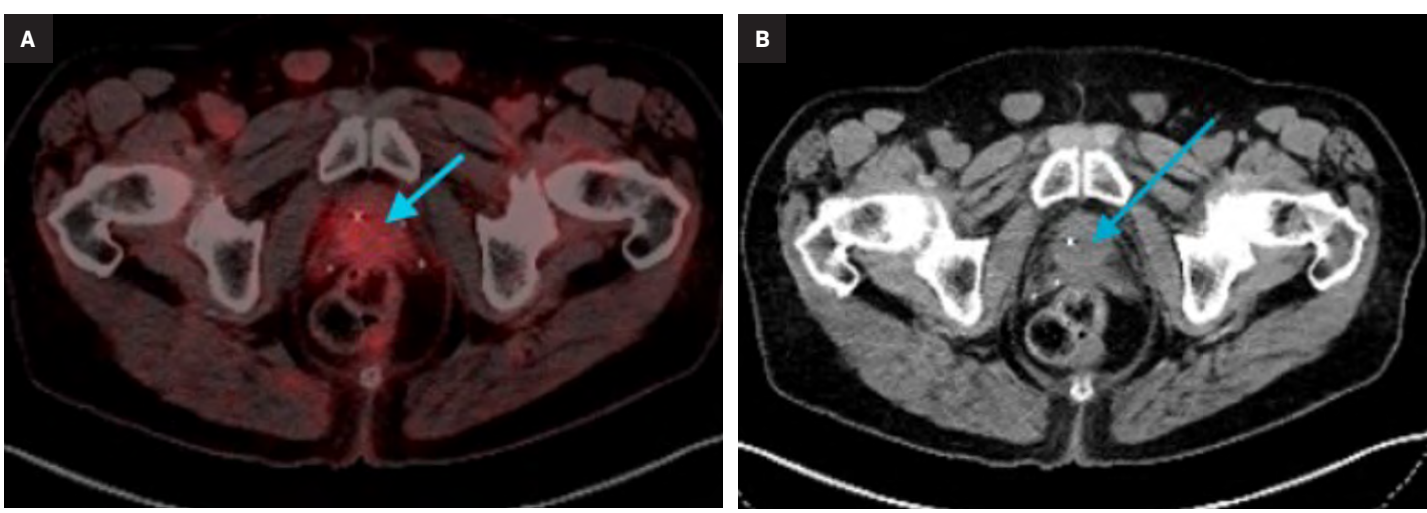


## Patient #2

A 73-year-old male with a BMI of 27.8 kg/m$^2$ and a history of unfavorable intermediate-risk prostate adenocarcinoma (clinical stage cT1c, PSA 5.4 ng/mL, Gleason score 3+4=7) underwent definitive external beam radiation therapy with concurrent ADT. Despite initial biochemical response, 4 years later, the patient's PSA increased from 0.05 ng/mL to 0.31 ng/mL while on apalutamide and degarelix; thus, $^{68}$Ga-PSMA-11 PET/CT (6.9 mCi; 76-minute uptake; 2.5 minutes/bed for 10 beds; total scan time 25 minutes) was conducted and demonstrated radiotracer uptake localized to the prostate, suggestive of intraprostatic recurrence (Figure 2). The patient's current management plan includes salvage stereotactic body radiation therapy (SBRT) to the prostate and a change in systemic therapy.

**Figure 3.** $^{68}$Ga-PSMA-11 PET/CT showing PSMA avid disease at the T12 vertebral level. (A) Transversal fused PET/CT, (B) sagittal fused PET/CT, and (C) CT.

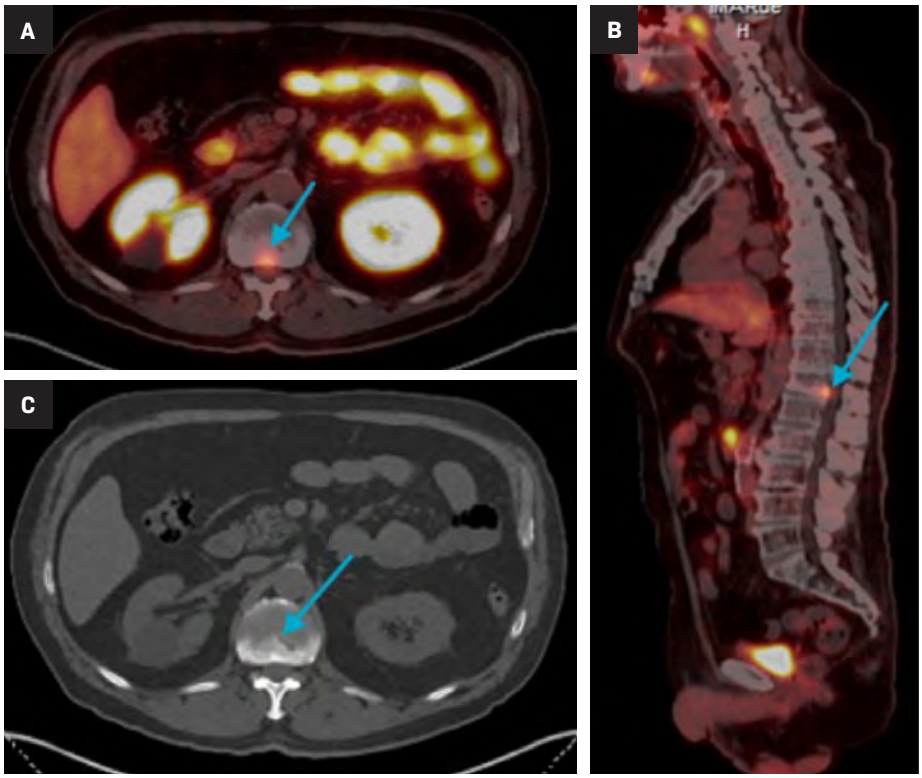


## Patient #3

A 75-year-old male with a BMI of >30 kg/m$^2$ and a history of high-risk prostate adenocarcinoma underwent RALP. Final pathology revealed pT3aN1 disease with a preoperative PSA of 7.4 ng/mL, Gleason score 4+4=8, positive lymph nodes, lymphovascular invasion, and positive surgical margins. Following biochemical recurrence, the patient was initiated on ADT. $^{68}$Ga-PSMA-11 PET/CT imaging demonstrated radiotracer uptake in both the prostate bed and spleen. He subsequently completed radiation therapy to both sites. Most recently, the patient's PSA, previously undetectable, increased to 0.19 ng/mL. Repeat $^{68}$Ga-PSMA-11 PET/CT (6.9 mCi; 54-minute uptake; 2.5 minutes/bed for 10 beds; total scan time 25 minutes) identified a new site of uptake at the T12 vertebral level (Figure 3). The current management plan includes SBRT to the T12 lesion.

**Figure 4.** $^{68}$Ga-PSMA-11 PET/CT showing PSMA avid disease in left external iliac lymph node. (A) Transversal fused PET/CT and (B) CT.

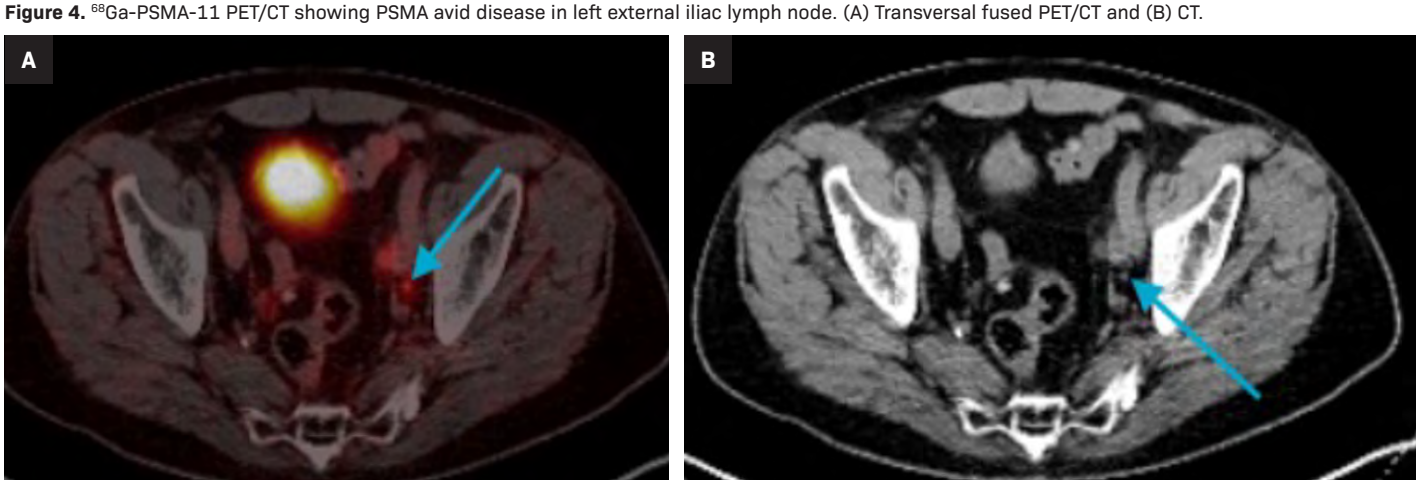


## Patient #4

A 77-year-old male with a BMI of 28.1 kg/m$^2$ and a history of high-risk prostate adenocarcinoma (clinical stage cT4N0M0, PSA 13.3 ng/mL, Gleason score 4+5=9) was initially treated with ADT and EBRT. He later developed locoregional recurrence involving the prostate gland and a single pelvic lymph node. Management included SBRT to the involved node in combination with continued ADT and the addition of darolutamide, with EBRT completed thereafter. Subsequently, his PSA, previously undetectable, increased to 0.05 ng/mL. $^{68}$Ga-PSMA-11 PET/CT (7.0 mCi; 65-minute uptake; 2.5 minutes/bed for 9 beds; total scan time 22.5 minutes) revealed new radiotracer uptake in a left external iliac lymph node (Figure 4). The current management plan includes a change in systemic therapy.

**Figure 5.** $^{68}$Ga-PSMA-11 PET/CT showing PSMA avid disease in right sixth rib. (A) Transversal fused PET/CT, (B) coronal fused PET/CT, and (C) CT.

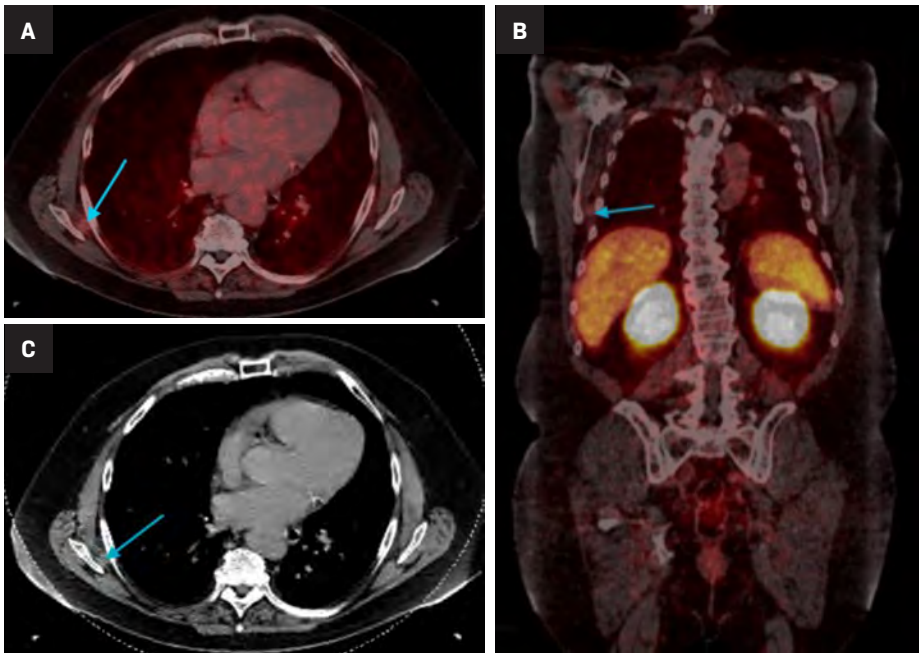


## Patient #5

A 70-year-old male with a BMI of 40 kg/m$^2$ and a history of prostate adenocarcinoma (pathologic stage pT2cN0, Gleason score 3+4=7) underwent RALP. He subsequently received salvage EBRT with ADT for biochemical recurrence. Five years later, he developed oligometastatic disease involving the T11 spine, which was treated with SBRT. His PSA has remained undetectable for over a year. The patient recently expressed interest in initiating testosterone supplementation. A precautionary $^{68}$Ga-PSMA-11 PET/CT (7.0 mCi; 56-minute uptake; 3.0 minutes/bed for 10 beds; total scan time 30 minutes) was performed, revealing radiotracer uptake in the right sixth rib (Figure 5). The current management plan includes SBRT to the identified site.

## Conclusion

Our case series highlights the clinical feasibility and diagnostic value of the best practice of administering 6 to 7 mCi of $^{68}$Ga-PSMA-11 to patients. We demonstrate high image quality on 16-year-old scanner technology in patients with low PSA levels and across a range of BMIs (25 to >40 kg/m$^2$). These real-world examples not only illustrate the flexibility of this dosing strategy across diverse body habitus but also highlights its potential to augment detection efficacy and impact clinical decision making.

Importantly, the increased administered activity appears to contribute to improved image quality by increasing number of coincidence counts,[7] which allows for the possibility to shorten scan duration and enhance patient comfort and overall experience. This has meaningful implications for clinical workflow efficiency, particularly in settings utilizing older PET technology where scan time and image resolution are often constrained.[9-12] By following the best practice of a 6 to 7 mCi dosing strategy for $^{68}$Ga-PSMA-11, institutions may achieve both clinical and cost-saving benefits.

## References

1) Illuccix (kit for the preparation of gallium Ga $^{68}$ gozetotide injection) prescribing information. Telix Pharmaceuticals; 2024.

2) Bryce AH, Agarwal N, Beltran H, et al. Implementing evidence-based strategies for men with biochemically recurrent and advanced prostate cancer: Consensus recommendations from the US Prostate Cancer Conference 2024. *Cancer.* Jan 1 2025;131(1):e35612. doi:10.1002/cncr.35612

*3) EAU Guidelines. Edn. presented at the EAU Annual Congress Madrid 2025.* ISBN 978-94-92671-29-5. 2025.

4) Gozellix (kit for the preparation of gallium Ga $^{68}$ gozetotide injection) prescribing information. Telix Pharmaceuticals; 2025.

5) Purysko AS, Abreu AL, Lin DW, Punnen S. Not all prostate-specific membrane antigen imaging agents are created equal: diagnostic accuracy of Ga-$^{68}$ PSMA-11 PET/CT for initial and recurrent prostate cancer. *Applied Radiology.* 2024.

6) Moses WW. Fundamental Limits of Spatial Resolution in PET. *Nucl Instrum Methods Phys Res A.* Aug 21 2011;648 Supplement 1:S236-s240. doi:10.1016/j.nima.2010.11.092

7) Karakatsanis NA, Fokou E, Tsoumpas C. Dosage optimization in positron emission tomography: state-of-the-art methods and future prospects. *Am J Nucl Med Mol Imaging.* 2015;5(5):527-47.

8) Rajapakse CS, Chang G. Impact of body habitus on radiologic interpretations. *Acad Radiol.* Jan 2014;21(1):1-2. doi:10.1016/j.acra.2013.10.006

9) Ataya M, Bahler CD, Koch M, et al. Can the sensitivity of prostate cancer with $^{68}$Ga-PSMA PET/CT improve with newer higher resolution PET-CT cameras? *J Urol.* 2025;213(5S):e1098.

10) Chen W, Li Y, Li Z, et al. Advantages and Challenges of Total-Body PET/CT at a Tertiary Cancer Center: Insights from Sun Yat-sen University Cancer Center. *J Nucl Med.* May 6 2024;65(Suppl 1):54S-63S. doi:10.2967/jnumed.123.266948

11) Vaquero JJ, Kinahan P. Positron Emission Tomography: Current Challenges and Opportunities for Technological Advances in Clinical and Preclinical Imaging Systems. *Annu Rev Biomed Eng.* 2015;17:385-414. doi:10.1146/annurev-bioeng-071114-040723

12) Surti S, Pantel AR, Karp JS. Total body PET: Why, how, what for? *TRPMS.* 2020;4(3):283-292. doi:10.1109/TRPMS.2020.2985403

13) Feder J. Medical equipment continues to age in the Unites States. *Radiology Oncology Systems.* Accessed 6 Feb, 2025. https://www.oncologysystems.com/blog/medical-equipment-continues-to-age-in-the-united-states/

14) Young L. IMV: PET/CT drivers PET scan volume to new heights. AuntMinnie.com. Accessed 6 Feb, 2025. https://www.auntminnie.com/clinical-news/molecular-imaging/article/15623310/imv-pet-ct-drives-pet-scan-volume-to-new-heights

15) Data from: Data on File. 6-7 mCi orders.2025.

REPRINTED FROM LOH 02-25
LEADERS ON THE HORIZON

# Diagnostic Accuracy of Cerebroplacental Ratio in Anticipating Adverse Perinatal Outcome in Uncomplicated Appropriate-for-Gestational-Age Pregnancies at Term

Abhijan Maity, MBBS; Bhawana Sonawane, MD; Anagha Deshpande, MD; Sunita Bhutada, MD

## Abstract

**Objectives and Hypothesis:** Anticipating which babies are in danger of experiencing poor outcomes during the perinatal period in uncomplicated appropriate-for-gestational-age (AGA) pregnancies at term is difficult in obstetric practice. Cerebroplacental ratio (CPR) is emerging as a significant indicator of negative perinatal results. The current study sought to establish the efficacy of CPR in predicting negative perinatal outcomes in term uncomplicated AGA pregnancies.

**Materials and Methods:** This was a hospital-based prospective observational cohort study conducted at a single center. Patients were chosen based on different criteria for inclusion and exclusion. A prenatal color Doppler US scan was carried out to calculate CPR. Patients were grouped into either normal CPR or pathological CPR categories based on their last CPR measurement before delivery. Doppler results did not impact clinical decisions, and delivery followed institutional protocols. After childbirth, data on the outcome of the perinatal period were obtained from the patients' medical records. Negative perinatal outcomes were assessed through the delivery method, APGAR score, perinatal morbidity, and perinatal mortality. These outcomes were correlated with CPR.

**Results:** The study included 605 women separated into normal and pathological CPR groups. Of these, 452 (74.7%) were assigned to the normal CPR category, and 153 (25.3%) were assigned to the pathological CPR category. In our study, 138 patients in the pathological CPR group experienced adverse perinatal outcomes, while 44 patients in the normal CPR group experienced adverse outcomes. The diagnostic accuracy of pathological CPR to predict any negative perinatal result was 90.25%.

**Conclusion:** The CPR shows potential in detecting at-risk fetuses in full-term uncomplicated AGA pregnancies.

**Keywords:** cerebroplacental ratio, appropriate for gestational age, adverse perinatal outcome, term uncomplicated pregnancy

## Introduction

A national, survey-based analysis published in 2023 found that 49.4% of Indian women experienced high-risk pregnancies, while 50.6% experienced low-risk pregnancies (LRPs).[1] Predicting whether a fetus is in danger of a negative perinatal outcome at term (37 weeks 0 days to 41 weeks 6 days of gestation) LRP is difficult. While high-risk pregnant women are promptly transferred from primary health care (PHC) to first referral unit (FRU) care, low-risk pregnant women, who make up the majority of those receiving antenatal care at PHC, frequently require

**Affiliation** Department of Radio-diagnosis, Indira Gandhi Government Medical College and Hospital, Nagpur, India.
**Disclosure:** The authors have no confli ts of interest to disclose. None of the authors received outside funding for the production of this original manuscript and no part of this article has been previously published elsewhere.

Published: February 1, 2025. https://doi.org/10.37549/AR-D-24-0061

immediate referral to FRU for intrapartum fetal distress. Women requiring immediate transfer to an FRU for emergency cesarean section (CS) typically experience worse perinatal outcomes than those who are promptly referred for elective CS.[2] Therefore, a screening tool is necessary to identify LRPs at risk of adverse perinatal outcomes, allowing for timely referral to FRU and thus ultimately reducing perinatal morbidity and mortality.

Although being small for gestational age (SGA; ie, fetuses with estimated fetal weight or EFW below the 10th percentile for gestational age) is a recognized risk factor for poor perinatal outcomes, most adverse outcomes actually involve fetuses that are appropriate for gestational age (AGA; ie, fetuses with EFW between the 10th and 90th percentiles).[3] Hence, relying solely on EFW may not accurately identify all fetuses at risk for adverse perinatal outcomes at term.

Recent studies have shown that some AGA fetuses have not reached their full genetic growth potential by the end of pregnancy and may experience negative outcomes during the perinatal period.[4] Detecting fetuses at risk of perinatal complications, particularly those in LRPs, is currently the main challenge in obstetric health care. In recent years, the cerebroplacental ratio (CPR) has become increasingly important as a predictor of negative outcomes. This has consequences for assessing the well-being of SGA and AGA fetuses close to the end of pregnancy.[5]

Calculated by dividing the Doppler flow rate of the middle cerebral artery (MCA) by the flow rate of the umbilical artery (UA), the CPR is an obstetric US measurement that demonstrates how elevated placental resistance and fetal hypoxia lead to the redistribution of cardiac output to the cerebral circulation. Owing to cerebral vasodilation and increased diastolic flow, this brain-sparing effect leads to a reduction in the pulsatility index (PI) of the MCA[6] and helps protect the brain from damage. Although other Doppler indices such as the systolic/diastolic ratio and resistance index have been used to calculate CPR in the past, PI is currently the preferred method for estimating the CPR.[7]

Fetal hypoxia leads to increased perinatal morbidity and mortality rates and is a key factor in various neurodevelopmental issues, hypoxic-ischemic encephalopathy, stillbirth, and other negative perinatal results worldwide.[8] During labor, fetal hypoxia is caused by uterine contractions and falling uterine artery flow velocities, resulting in decreased placental perfusion.[9] Blood vessels in the brain react with vasodilation, decreasing resistance to blood flow and resulting in a lower PI in MCA.[10]

The majority of clinical research into the CPR has centered on evaluating complicated pregnancies. Little research has been conducted on how CPR is involved in evaluating pregnancies with no or low risk for complications. Our study aimed to assess how well CPR can predict adverse perinatal outcomes in term uncomplicated or low-risk AGA pregnancies.

## Materials and Methods

This was a single-center, hospital-based prospective observational cohort study. Cases were chosen from among pregnant women being referred to our institution's Department of Radio-Diagnosis for antenatal color Doppler US scanning. The 2-year study was conducted between January 2022 and December 2023.

In addition to giving informed consent, participants in the study had to meet specific criteria for eligibility: (1) term pregnancy (37 weeks 0 days, or 259 days, to 41 weeks 6 days, or 293 days of gestation); (2) singleton pregnancy; (3) confirmed gestational age (based on crown-rump length measurement between 6 and 12 weeks of gestation); (4) nulliparous or previous normal vaginal delivery; (5) be between 20 and 35 years of age; (6) cephalic presentation; (7) normal amniotic fluid index (AFI, between 5 and 25 cm); and (8) AGA pregnancies (EFW between the 10th and 90th percentiles for the gestational age).

In addition to refusal to give informed consent, subjects were excluded for (1) preterm delivery (<37 weeks or <259 days of gestation); (2) post-term pregnancy (≥42 weeks 0 days, or 294 days); (3) twin or multiple pregnancies; (4) unconfirmed gestational age; (5) being below age 20 or above 35; (6) known fetal anomalies; (7) intrauterine fetal demise; (8) medical or surgical illnesses complicating pregnancy (eg, pregnancy-induced hypertension, preeclampsia, hypothyroidism, gestational diabetes mellitus, severe anemia, syphilis/HIV positive, and so forth); (9) Rh-negative; (10) poor obstetric history; (11) malpresentation; (12) low-lying placenta/placenta previa; (13) oligohydramnios (AMI < 5 cm) or polyhydramnios (AFI > 25 cm); (14) previous CS or uterine surgery such as myomectomy; (15) elective CS; (16) emergency CS for reasons other than intrapartum fetal compromise (IFC); and (17) SGA (EFW below the 10th percentile for the gestational age) or LGA (EFW above the 90th percentile for the gestational age) pregnancies.

The research was carried out according to the Declaration of Helsinki and received ethical approval from the institution's ethics committee. During their


https://doi.org/10.37549/AR-D-24-0061

initial appointment, patients were asked to give written consent in their native language before undergoing a thorough history and clinical examination. The evaluation included information about the mother's age, previous pregnancies, estimated gestational age from the last menstrual period, menstrual cycle and obstetric history, past or current medical conditions, surgical history, medication use or allergies, smoking habits, alcohol consumption, and tobacco use. The clinical assessment covered blood pressure, body mass index, and a general survey evaluation.

Each subject then underwent an antenatal color Doppler US scan for CPR calculation; this procedure was performed every 8 days until delivery to ensure Doppler values were current within 7 days of delivery. The final CPR before delivery was utilized for all examinations.

A single US machine, the Mindray DC 80, equipped with a Mindray SC6-1E transabdominal curved array transducer with a frequency range of 1.3-5.7 MHz, was used for all US procedures. An obstetric scanning guideline recommended by the US Food and Drug Administration was followed, keeping the spatial peak temporal average intensity below 94 mW/cm$^2$. Smart Care US gel was applied for transmission of the US.

The gestational age was verified by measuring the crown-rump length between 6 and 12 weeks of pregnancy. Fetal biometry and AFI were documented during every appointment. The EFW was determined using the Hadlock formula incorporating biparietal diameter, head and abdominal circumference, and femur length.[11] Fetuses with EFW below the 10th percentile for gestational age were classified as SMA, and those with EFW between the 10th and 90th percentile were classified as AGA.[12]

Doppler parameters were assessed based on the revised guidelines set by the International Society of Ultrasound in Obstetrics and Gynecology (ISUOG).[13] Doppler assessment of the UA was performed from a loose loop of the umbilical cord located away from the insertion sites of the placenta or the fetus. Assessment of the MCA was conducted by observing a cross-sectional image of the fetal head at the trans-thalamic plane, which includes the thalami and cavum septum pellucidum. MCA Doppler was evaluated in the circle of Willis in the straight part of the artery about 1 cm away from its origin at the internal carotid artery.

Efforts were made to avoid undue transducer compression on the fetal head, which can change intracranial pressure and affect Doppler assessment of the MCA. Two skilled radiologists recorded all Doppler waveforms while the patient was lying supine with the head of the bed raised at a 45° angle. The CPR was determined by dividing the MCA PI by the UA PI and utilizing reference ranges based on gestational age instead of relying on a single threshold. The CPR was assessed as either normal or abnormal using the calculator found at https://portal.medicinafetalbarcelona.org/calc/.[14]

Subjects were separated into 2 groups based on their last CPR measurement before delivery: one with normal CPR and the other with pathological CPR. The results from Doppler tests were not utilized in the treatment plan. Patients and obstetricians were unaware of the CPR outcomes. Labor and childbirth were conducted according to institutional protocols and guidelines. Post delivery, information on perinatal outcomes was retrieved from the patient's medical records.

Adverse perinatal outcomes were assessed through the mode of delivery (including instrumental deliveries or CS for IFC; diagnosis of IFC was determined by cardiotocographic abnormalities, fetal heart sound irregularities, meconium stained liquor, or a combination of these); APGAR scores < 7 at 5 minutes; perinatal morbidity (admission to the neonatal intensive care unit [NICU] within 24 hours post delivery); and perinatal mortality (including stillbirth and death within the first week of life). The CPR was correlated with negative outcomes during childbirth.

## Statistical Analysis

The data gathered were inputted into a Microsoft Excel spreadsheet designed for Windows 10. Statistical Package for Social Sciences Version 22.0 (SPSS Inc., Chicago, Illinois, USA) software was used for statistical analysis, upon which the results were displayed in tables. Quantitative data were represented in numbers and percentages and presented as mean ± SD. Nonparametric tests such as the chi-square test were employed to test the significance of difference for qualitative data, and parametric tests such as independent *t* tests were performed to assess the significance of difference for quantitative data. Tests for diagnostic accuracy were performed by measuring sensitivity, specificity, positive predictive value (PPV), negative predictive value (NPV), positive likelihood ratio (positive LR), negative likelihood ratio (negative LR), area under receiver operating characteristic (ROC) curve (AUC-ROC), and overall diagnostic accuracy within a 95% CI. Any

**Table 1. Baseline Characteristics of Study Population, *N* = 605**

| BASELINE CHARACTERISTICS | NORMAL CEREBROPLACENTAL RATIO (*N* = 452) | PATHOLOGICAL CEREBROPLACENTAL RATIO (*N* = 153) | *P* VALUE |
|---|---|---|---|
| Maternal age[a] (years) | 26.97±4.32 | 27.11±4.3 | .73[c] |
| Gestational age at time of last Doppler scan[a] (days) | 273.11±7.7 | 273.66±7.45 | .44[c] |
| Gestational age at time of delivery[a] (days) | 277.15±7.54 | 277.75±7.28 | 1.0[c] |
| Interval between last scan and delivery[a] (days) | 4.09±1.89 | 4.09±1.87 | .39[c] |
| Residency[b] (% of patients) | | | .37[d] |
| Rural | 244 (54) | 89 (58) | |
| Urban | 208 (46) | 64 (42) | |
| Literacy[b] (% of patients) | | | .68[d] |
| Illiterate | 105 (23) | 38 (25) | |
| Literate | 347 (77) | 115 (75) | |
| Parity[b] (% of patients) | | | .98[d] |
| Nulliparous | 261 (58) | 87 (57) | |
| Primiparous | 145 (32) | 50 (33) | |
| Multiparous | 46 (10) | 16 (10) | |

[a]*The data are given as the mean ± SD.*

[b]*The data are given as the number (%) of patients.*

[c]*Independent-sample Student t test.*

[d]$\chi^2$ *test.*

probability value (*P* value) <.05 was deemed statistically significant with a 95% CI.

## Results

In the study period, 627 women were deemed eligible for the study, with 12 women excluded from planned C-sections and 10 who were lost to follow-up. The ultimate group of participants included 605 female individuals. Of the 605 subjects, 452 (74.7%) were classifed as having normal CPR, while 153 (25.3%) were classified to the pathological CPR group.

The study population's baseline characteristics were recorded. There was no notable discrepancy between the 2 groups in maternal age, parity, literacy, residency, average gestational age at delivery, average gestational age at the last Doppler scan, and the average interval between the final Doppler scan and delivery, as demonstrated in Table 1.

As presented in Table 2, of the 153 subjects with pathological CPR, 138 (90.2%) experienced adverse perinatal outcomes, while among the 452 patients with normal CPR, only 44 (9.73%) had adverse perinatal outcomes, which was statistically significant (*P*<.00001).

Table 3 demonstrates that the rates of CS and instrumental deliveries for IFC, NICU admission within 24 hours of delivery, and an APGAR score < 7 at 5 minutes were notably elevated in the group with abnormal CPR compared with those with normal CPR. This was deemed to be statistically significant (*P*<.05).

Table 4 presents the diagnostic precision of pathological CPR in predicting adverse perinatal outcomes, as well as different types of adverse perinatal outcomes. The sensitivity, specificity, PPV, NPV, AUC, and overall diagnostic accuracy of pathological CPR to predict any adverse perinatal outcome were 75.82%, 96.45%, 90.2%, 90.27%, 0.86%, and 90.25%, respectively. Table 4 shows that CPR has high sensitivity, specificity, PPV, NPV, positive LR, AUC-ROC, and overall diagnostic accuracy and low negative LR for predicting any adverse perinatal outcome and also for predicting various adverse perinatal outcomes.

## Discussion

Determining which pregnant patients will experience a poor perinatal outcome during labor has always been a challenging task. Therefore, there is a need for a screening tool that can anticipate negative perinatal results beforehand. The CPR, which considers fetal response (MCA PI) and placental perfusion (UA PI), is increasingly being used to efficiently identify at-risk fetuses. The results of



https://doi.org/10.37549/AR-D-24-0061

**Table 2. Association of Cerebroplacental Ratio with Any Adverse Perinatal Outcome**

| | NORMAL CEREBROPLACENTAL RATIO (*N* = 452) | PATHOLOGICAL CEREBROPLACENTAL RATIO (*N* = 153) | *P* VALUE |
|---|---|---|---|
| Any adverse perinatal outcome[a] (% of patients) | | | <.00001[b] |
| Yes | 44 (10) | 138 (90) | |
| No | 408 (90) | 15 (10) | |

[a]*The data are given as the number (%) of patients.*

[b]$\chi^2$ *test.*

https://doi.org/10.37549/AR-D-24-0061

**Table 3. Association of Cerebroplacental Ratio with Various Adverse Perinatal Outcomes**

| ADVERSE PERINATAL OUTCOMES | NORMAL CEREBROPLACENTAL RATIO (*N* = 452) | PATHOLOGICAL CEREBROPLACENTAL RATIO (*N* = 153) | *P* VALUE |
|---|---|---|---|
| Cesarean section for [a]intrapartum fetal compromise (% of patients) | 24 (5) | 105 (70) | <.00001[b] |
| Instrumental delivery for [a]intrapartum fetal compromise (% of patients) | 2 (0.4) | 9 (6) | <.001[c] |
| APGAR score < 7 at 5 minutes[a] (% of patients) | 6 (1.3) | 33 (22) | <.000001[c] |
| Admission to neonatal intensive care unit within 24 hours of delivery[a] (% of patients) | 18 (4) | 66 (44) | <.00001[b] |

[a]*The data are given as the number (%) of patients.*

[b]$\chi^2$ *test.*

[c]*Fisher exact test.*

our research show that conducting fetal CPR measurements in term, low-risk AGA pregnancies can predict an unfavorable perinatal outcome.

The present study found that in pregnancies with AGA babies, those with abnormal CPR had significantly higher rates of CS and instrumental delivery compared with those with normal CPR. This finding aligned with Khalil et al,[4] who showed a higher rate of CSs and instrumental deliveries for IFC in AGA pregnancies with poor CPR compared with normal CPR (11.0% vs 8.7%, *P*=.043% and 11.2% vs 7.8%, *P*=.003, respectively).

We found that 44% of the infants in the low-CPR group required NICU hospitalization, in contrast to 4% of those in the normal CPR group (*P*<.05). Flood et al[15] also found that pathological CPR was associated with a higher requirement for infant NICU hospitalization compared with those in the normal CPR group (69.4% vs 22%, *P*<.0001). Prior et al[16] also reported that the pathological group had higher NICU admission rates, but this difference was not statistically significant.

Our study also observed a higher percentage of infants with low APGAR scores in the pathological CPR group; 22% of infants in this group had an APGAR score below 7 at 5 minutes compared with 1.3% of infants in the normal CPR group with an APGAR score below 7 (*P*<.0001). This aligns with findings by Ropacka Lesiak et al[17] and Gramellini et al,[18] who observed a higher incidence of infants with low APGAR scores in the abnormal CPR group. No cases of perinatal mortality were documented in either group in our study.

To summarize, we observed an increased rate of cesarean and instrumental deliveries in pregnancies with pathological CPR compared with normal CPR, as well as higher NICU admission and poorer APGAR scores for infants. This comports with similar findings by Mohamed et al[19] and Anand et al,[20] who reported higher rates of cesarean and instrumental delivery for IFC, NICU admission, and babies with poor APGAR score in term uncomplicated AGA pregnancies with low CPR compared with normal CPR.

The results strongly suggest that negative perinatal outcomes are associated with abnormal CPR in term, low-risk pregnancies. Currently, routine Doppler tests are not recommended for fetuses with normal EFW. A 2010 Cochrane systematic review database suggests there is not enough evidence to show that using fetal Doppler in low-risk term AGA pregnancies can reduce the rates of perinatal morbidity and mortality.[21]

**Table 4. Diagnostic Accuracy of Pathological Cerebroplacental Ratio for Predicting Any Adverse Perinatal Outcome**

| DIAGNOSTIC ACCURACY | ANY ADVERSE PERINATAL OUTCOME | CESAREAN SECTION FOR INTRAPARTUM FETAL COMPROMISE | INSTRUMENTAL DELIVERY FOR INTRAPARTUM FETAL COMPROMISE | APGAR SCORE < 7 AT 5 MINUTES | ADMISSION TO NEONATAL INTENSIVE CARE UNIT WITHIN 24 HOURS OF DELIVERY |
|---|---|---|---|---|---|
| Sensitivity (95% CI) | 75.82 (68.94-81.85) | 81.4 (73.59-87.7) | 81.82 (48.22-97.72) | 84.62 (69.47-94.14) | 78.57 (68.26-86.78) |
| Specificit (95% CI) | 96.45 (94.22-98) | 89.92 (73.59-87.2) | 75.76 (72.1-79.15) | 78.8 (75.2-82.1) | 83.3 (79.82-86.4) |
| Positive predictive value (95% CI) | 90.2 (84.75-93.84) | 68.63 (62.29-74.33) | 5.88 (4.37-7.87) | 21.57 (18.26-25.29) | 43.14 (37.8-48.6) |
| Negative predictive value (95% CI) | 90.27 (87.75-92.31) | 94.69 (92.54-96.24) | 99.56 (98.47-99.87) | 98.67 (97.26-99.36) | 96.02 (94.11-97.32) |
| Positive likelihood ratio (95% CI) | 21.38 (12.92-35.39) | 8.07 (6.1-10.69) | 3.37 (2.47-4.61) | 3.99 (3.24-4.91) | 4.7 (3.77-5.87) |
| Negative likelihood ratio (95% CI) | 0.25 (0.19-0.32) | 0.21 (0.14-0.3) | 0.24 (0.07-0.84) | 0.19 (0.09-0.41) | 0.26 (0.17-0.39) |
| Area under receiver operating characteristic curve (95% CI) | 0.86 (0.83-0.89) | 0.86 (0.83-0.88) | 0.79 (0.75-0.82) | 0.82 (0.78-0.85) | 0.81 (0.78-0.84) |
| Overall diagnostic accuracy (95% CI) | 90.25 (87.6-92.49) | 88.1 (85.25-90.57) | 75.87 (72.25-79.23) | 79.17 (75.72-82.34) | 82.65 (79.39-85.58) |

Most previous research has focused mainly on the predictive value of CPR for adverse perinatal outcomes in SGA fetuses and high-risk or complicated pregnancies.[15,17,22-25] However, many current studies indicate that AGA fetuses with abnormal CPR are linked to a heightened risk of negative perinatal outcomes.[4,7,16,19,20,26-28] Therefore, it is feasible to include regular, late-third-trimester CPR measurement in routine clinical practice to detect at-risk AGA fetuses who may suffer from placental insufficiency and fail to reach their full genetic potential at term as they may not be identified as high risk through traditional methods such as EFW. Our study adds to the growing body of evidence indicating that abnormal CPR in SGA and AGA pregnancies is a separate indicator of a negative perinatal outcome.

Debate continues regarding the best CPR cut-off value to identify negative perinatal outcomes. Recent research has used percentiles (<5 th or 10th percentile)[7,16,29-31] or multiple of median[32]; on the other hand, earlier studies used absolute values (<1[15,20,28] or <1.08[17,18] or <1.1).[19] Instead of utilizing one specific CPR cut-off value, we determine CPR by considering reference ranges associated with gestational age, as per the latest ISUOG practice guidelines.[14] Our research demonstrated a sensitivity of 75.82%, specificity of 96.45%, PPV of 90.2%, NPV of 90.27%, AUC of 0.86%, and an overall diagnostic accuracy of 90.25% for predicting adverse perinatal outcomes with CPR in the study population. As a result, we believe that CPR using gestational age-specific reference ranges is more strongly linked to adverse perinatal outcome than is a single cut-off value.

Our study suggests CPR measurement should be incorporated into standard practice for term uncomplicated or low-risk AGA pregnancies. This can help identify pregnancies requiring advanced care with facilities for continuous electronic fetal monitoring (EFM), emergency CS, and NICU, in contrast to those with normal CPR that can be managed without such capabilities. Therefore, our study findings align with those of most previous studies that focused on the same important clinical question.

### Strengths of the Study

Obstetricians are unaffected by the CPR; thus, the measurement will not impact clinical decision-making regarding delivery. Additionally, based on what we know as of now, few studies have been conducted



https://doi.org/10.37549/AR-D-24-0061

on the efficacy of CPR in predicting negative perinatal outcomes in term uncomplicated AGA pregnancies. Of these, most are retrospective in nature.[4,7,26-28] While some prospective studies have been completed,[16,19,20] ours has the largest number of study groups. Furthermore, all the previous prospective studies utilized only one CPR cut-off value, whereas ours utilized the most recent ISUOG guideline for CPR calculation.[14]

### Limitations of the Study

Currently, because there are not enough color Doppler facilities in rural areas, many pregnant women in these regions cannot be screened for the CPR. Furthermore, to date there is a lack of properly structured prospective, randomized, controlled trials regarding the efficacy of CPR in predicting negative perinatal outcomes in low-risk, uncomplicated term AGA pregnancies. Hence, before incorporating routine CPR measurement into clinical practice, a well-planned, prospective, randomized, controlled study involving a larger population is needed. Additionally, we did not incorporate umbilical cord blood gas analysis in our study, which may have shown a stronger correlation with negative perinatal outcomes.

## Conclusion

Measuring the CPR appears to be a highly encouraging technique for recognizing at-risk fetuses. Owing to the decreasing costs of US machines, measuring the CPR in full-term pregnancies can become a routine clinical practice that can be performed quickly and accurately by a trained medical professional during third-trimester, antepartum evaluations. Through the CPR, at-risk pregnancies can be identified in advance, assisting health care professionals in making more-informed decisions and timely referrals to higher level facilities, ultimately enhancing perinatal results.

Because of the CPR's high sensitivity, specificity, AUC, PPV, NPV, and diagnostic accuracy, women with normal values can likely give birth at local facilities with limited resources as the risk for complications is minimal in such cases. Conversely, women with abnormal CPRs and increased likelihood of complications for their babies can be promptly transferred to a more advanced center with continuous EFM, emergency CS, and NICU capabilities.

## References

1) Kuppusamy P, Prusty RK, Kale DP. High-risk pregnancy in india: prevalence and contributing risk factors—a national survey-based analysis. *J Glob Health*. 2023;13(13):04116. doi:10.7189/jogh.13.04116

2) Benzouina S, Boubkraoui ME-M, Mrabet M, et al. Fetal outcome in emergency versus elective cesarean sections at souissi maternity hospital, Rabat, Morocco. *Pan Afr Med J*. 2016;23(23):197. doi:10.11604/pamj.2016.23.197.7401

3) Khalil A, Thilaganathan B. Role of uteroplacental and fetal doppler in identifying fetal growth restriction at term. *Best Pract Res Clin Obstet Gynaecol*. 2017;38:38-47. doi:10.1016/j.bpobgyn.2016.09.003

4) Khalil AA, Morales-Rosello J, Morlando M, et al. Is fetal cerebroplacental ratio an independent predictor of intrapartum fetal compromise and neonatal unit admission?. *Am J Obstet Gynecol*. 2015;213(1):54. doi:10.1016/j.ajog.2014.10.024

5) DeVore GR. The importance of the cerebroplacental ratio in the evaluation of fetal well-being in SGA and AGA fetuses. *Am J Obstet Gynecol*. 2015;213(1):5-15. doi:10.1016/j.ajog.2015.05.024

6) Ebrashy A, Azmy O, Ibrahim M, Waly M, Edris A. Middle cerebral/umbilical artery resistance index ratio as sensitive parameter for fetal well-being and neonatal outcome in patients with preeclampsia: case-control study. *Croat Med J*. 2005;46(5):821-825.

7) Morales-Roselló J, Khalil A, Morlando M, et al. Changes in fetal doppler indices as a marker of failure to reach growth potential at term. *Ultrasound Obstet Gynecol*. 2014;43(3):303-310. doi:10.1002/uog.13319

8) Blencowe H, Cousens S, Jassir FB, et al. National, regional, and worldwide estimates of stillbirth rates in 2015, with trends from 2000: a systematic analysis. *Lancet Glob Health*. 2015;4(2):e98-e108.

9) Low JA, Pickersgill H, Killen H, Derrick EJ. The prediction and prevention of intrapartum fetal asphyxia in term pregnancies. *Am J Obstet Gynecol*. 2001;184(4):724-730. doi:10.1067/mob.2001.111720

10) Bligh LN, Alsolai AA, Greer RM, Kumar S. Cerebroplacental ratio thresholds measured within 2 weeks before birth and risk of cesarean section for intrapartum fetal compromise and adverse neonatal outcome. *Ultrasound in Obstet & Gyne*. 2018;52(3):340-346. doi:10.1002/uog.17542

11) Hadlock FP, Harrist RB, Sharman RS, Deter RL, Park SK. Estimation of fetal weight with the use of head, body, and femur measurements--a prospective study. *Am J Obstet Gynecol*. 1985;151(3):333-337. doi:10.1016/0002-9378(85)90298-4

12) Salomon LJ, Alfirevic Z, Da Silva Costa F, et al. ISUOG practice guidelines: ultrasound assessment of fetal biometry and growth. *Ultrasound Obstet Gynecol*. 2019;53(6):715-723. doi:10.1002/uog.20272

13) Bhide A, Acharya G, Baschat A, et al. ISUOG practice guidelines (updated): use of doppler velocimetry in obstetrics. *Ultrasound Obstet Gynecol*. 2021;58(2):331-339. doi:10.1002/uog.23698

14) Ciobanu A, Wright A, Syngelaki A, et al. Fetal medicine foundation reference ranges for umbilical artery and middle cerebral artery pulsatility index and cerebroplacental ratio. *Ultrasound in Obstet & Gyne*. 2019;53(4):465-472. doi:10.1002/uog.20157

15) Flood K, Unterscheider J, Daly S, et al. The role of brain sparing in the prediction of adverse outcomes in intrauterine growth restriction: results of the multicenter PORTO study. *Am J Obstet Gynecol*. 2014;211(3):288. doi:10.1016/j.ajog.2014.05.008

16) Prior T, Mullins E, Bennett P, Kumar S. Prediction of intrapartum fetal compromise using the cerebroumbilical ratio: a prospective observational study. *Am J Obstet Gynecol*. 2013;208(2):124. doi:10.1016/j.ajog.2012.11.016

17) Ropacka-Lesiak M, Korbelak T, Świder-Musielak J, Breborowicz G. Cerebroplacental ratio in prediction of adverse perinatal outcome and fetal heart rate disturbances in uncomplicated pregnancy at 40 weeks and beyond. *Arch Med Sci*. 2015;11(1):142-148. doi:10.5114/aoms.2015.49204

18) Gramellini D, Folli MC, Raboni S, Vadora E, Merialdi A. Cerebral-umbilical doppler ratio as a predictor of adverse perinatal outcome. *Obstet Gynecol*. 1992;79(3):416-420. doi:10.1097/00006250-199203000-00018

19) Mohamed ML, Mohamed SA, Elshahat AM. Cerebroplacental ratio for prediction of adverse intrapartum and neonatal outcomes in a term uncomplicated pregnancy. *Middle East Fertil Soc J*. 2021;26(1):45. doi:10.1186/s43043-021-00090-3

20) Anand S, Mehrotra S, Singh U, Solanki V, Agarwal S. Study of association of fetal cerebroplacental ratio with adverse perinatal outcome in uncomplicated term AGA pregnancies. *J Obstet Gynaecol India*. 2020;70(6):485-489. doi:10.1007/s13224-020-01357-x

21) Alfirevic Z, Stampalija T, Gyte GM. Fetal and umbilical doppler ultrasound in normal pregnancy. *Cochrane Database Syst Rev*. 2015;4:CD001450.

22) Odibo AO, Riddick C, Pare E, Stamilio DM, Macones GA. Cerebroplacental doppler ratio and adverse perinatal outcomes in intrauterine growth restriction: evaluating the impact of using gestational age-specific reference values. *J Ultrasound Med*. 2005;24(9):1223-1228. doi:10.7863/jum.2005.24.9.1223

23) Bahado-Singh RO, Kovanci E, Jeffres A, et al. The doppler cerebroplacental ratio and perinatal outcome in intrauterine growth restriction. *Am J Obstet Gynecol*. 1999;180(3 pt 1):750-756. doi:10.1016/s0002-9378(99)70283-8

24) Alanwar A, El Nour AA, El Mandooh M, et al. Prognostic accuracy of cerebroplacental ratio for adverse perinatal outcomes in pregnancies complicated with severe pre-eclampsia; a prospective cohort study. *Pregnancy Hypertens*. 2018;14:86-89. doi:10.1016/j.preghy.2018.08.446

25) Malik N, Jain S, Ranjan R, et al. Cerebroplacental ratio as a predictor of perinatal outcome in hypertensive disorders of pregnancy and its comparison with its constituent doppler indices. *Cureus*. 2023;15(12):e49951. doi:10.7759/cureus.49951

26) Mecke L, Ignatov A, Redlich A. The importance of the cerebroplacental ratio for the prognosis of neonatal outcome in AGA fetuses. *Arch Gynecol Obstet*. 2023;307(1):311-317. doi:10.1007/s00404-022-06596-z

27) Ortiz JU, Graupner O, Flechsenhar S, et al. Prognostic value of cerebroplacental ratio in appropriate-for-gestational-age fetuses before induction of labor in late-term pregnancies. *Ultraschall Med*. 2023;44(1):50-55. doi:10.1055/a-1399-8915

28) Singh A, Lnu S, Bano I, Ahmad I. Doppler cerebroplacental ratio and adverse perinatal outcome. *Journal of South Asian Federation of Obstetrics and Gynaecology*. 2014;6(1):25-27. doi:10.5005/jp-journals-10006-1262

29) Berkley E, Chauhan SP, Abuhamad A, Society for Maternal-Fetal Medicine Publications Committee. Doppler assessment of the fetus with intrauterine growth restriction. *Am J Obstet Gynecol*. 2012;206(4):300-308. doi:10.1016/j.ajog.2012.01.022

30) Flatley C, Kumar S. Is the fetal cerebroplacental ratio better that the estimated fetal weight in predicting adverse perinatal outcomes in a low risk cohort?. *Journal of Maternal-Fetal & Neonatal Medicine*. 2019;32(14):2380-2386. doi:10.1080/14767058.2018.1438394

31) Bligh LN, Alsolai AA, Greer RM, Kumar S. Cerebroplacental ratio thresholds measured within 2 weeks before birth and risk of cesarean section for intrapartum fetal compromise and adverse neonatal outcome. *Ultrasound Obstet Gynecol*. 2018;52(3):340-346. doi:10.1002/uog.17542

32) Khalil A, Morales-Rosello J, Khan N, et al. Is cerebroplacental ratio a marker of impaired fetal growth velocity and adverse pregnancy outcome?. *Am J Obstet Gynecol*. 2017;216(6):606. doi:10.1016/j.ajog.2017.02.005



https://doi.org/10.37549/AR-D-24-0061

REPRINTED FROM LOH 02-25
LEADERS ON THE HORIZON

# Ankle Impingement Syndromes: What the Radiologist Needs to Know

Hira Qureshi, MD; Alex Sobotie, MD; Alexander Hallwachs, MD; Kacey Pagano, MD; Robert DeVita, MD; Richard Barger, MD; Vijaya Kosaraju, MD; Shana Miskovsky, MD; Navid Faraji, MD

Ankle impingement syndromes (AISs) compress the osseous and soft-tissue structures about the tibiotalar joint as a sequela of acute traumatic injury or repetitive microtrauma. They typically affect athletes who present with ankle pain and swelling that are relieved with rest. A chronic course may ensue with signs of ankle instability and/or limited range of motion (ROM), along with pain while squatting, sprinting, and climbing stairs. AISs are classified according to their location relative to the joint: anterior, anterolateral, anteromedial, posteromedial, or posterior.

While diagnosis is typically made with clinical examination, imaging plays an important role in localizing pathology and guiding treatment options, including surgery. Here, we review the anatomy, pathophysiology, physical exam, imaging characteristics, and management of AISs.

## Anatomy Overview

A basic understanding of ankle anatomy is integral to understanding the structures that may be involved in the various impingement syndromes.

The tibiotalar joint comprises the articulation of the tibia, fibula, and talus (Figure 1). The tibia and fibula collectively form a mortise that houses the trochlea of the talus, while the tibia forms the medial malleolus and the fibula forms the lateral malleolus. The malleoli constrain the talus into essentially a hinge joint with inherent stability in neutral alignment. Together with the wider anterior geometry of the talar trochlea, this imparts stability to the joint such that the bony constraints resist eversion in standing alignment. However, as the joint moves through the arc of motion along its oblique axis, the soft tissues become critical in maintaining ankle stability.

The syndesmotic complex restrains motion between the distal tibia and fibula to maintain the bony mortise geometry through dynamic motion. The complex comprises the anterior tibiofibular ligament (AITFL), posterior tibiofibular ligament, and the interosseous ligament. This complex is also referred to as the "high-ankle ligaments."

Inferior to these structures are the "low-ankle ligaments," including the deltoid ligament complex and the lateral ligament complex. The medial aspect of the ankle is supported by the former, which spans the medial malleolus to the calcaneus, navicular, and talus, and consists of a superficial and a deep layer. The superficial layer consists of the tibiocalcaneal, tibionavicular, and superficial posterior tibiotalar ligaments (PTTLs). The anterior tibiotalar (ATTL) and PTTL make up the deep layer (Figure 1). The deltoid ligamentous complex has a wide range of anatomical variations.[1]

The lateral ligament complex consists of 3 ligaments: anterior talofibular ligament (ATFL), calcaneofibular ligament (CFL), and posterior talofibular ligament (PTFL). The ATFL and PTFL attach the talus to the fibula anteriorly and posteriorly, respectively, while the CFL attaches the calcaneus to the fibula (Figure 1).

## Anterior Impingement

### Pathophysiology

The primary mechanism of anterior impingement syndrome is direct and/or repetitive microtrauma between the anterior tibial joint line and talar neck, resulting in the formation of osseous spurs.[2,3] These spurs can entrap soft tissue, causing acute swelling

**Affiliations:** Department of Radiology, Henry Ford Hospital, Detroit, Michigan (Qureshi). Department of Internal Medicine, University Hospital Cleveland Medical Center, Cleveland, Ohio (Sobotie). Department of Orthopedic Surgery, University Hospital Cleveland Medical Center, Cleveland, Ohio (Hallwachs, Miskovsky). Northeast Ohio Medical University, Rootstown, Ohio (Pagano). Department of Radiology, Medical University of South Carolina, Charleston, South Carolina (DeVita). Department of Radiology, University Hospital Cleveland Medical Center, Cleveland, Ohio (Barger, Kosaraju, Faraji).
**Disclosure:** The authors have no conflicts of interest to disclose. None of the authors received outside funding for the production of this original manuscript and no part of this article has been previously published elsewhere.

Published: February 1, 2025. https://doi.org/10.37549/AR-D-24-0064

**Figure 1.** From left to right: frontal, posteromedial, and lateral depictions of relevant ankle joint anatomy created on complete anatomy.

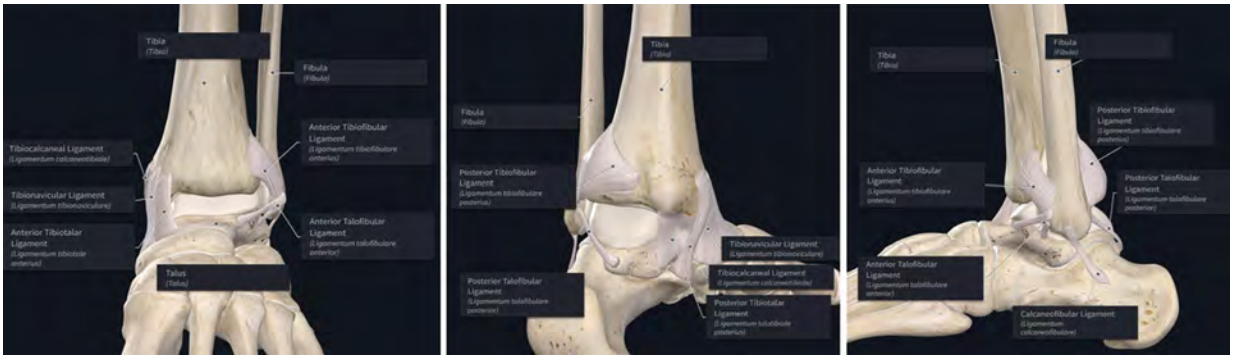


or long-term development of hypertrophic synovial plicae or adhesions and degenerative sequelae that further limit motion.[4,5]

### Physical Exam

Palpating the anterior joint line in slight plantarflexion may reveal tenderness over the ankle anterior to bony osteophytes. The anterior impingement test involves hyperdorsiflexion of the joint, eliciting tenderness across the front of the ankle.[6-8] Generally, patients may sustain loss of dorsiflexion ROM compared with the contralateral side. The Silfverskiöld test is also performed to rule out isolated gastrocnemius contracture, which can also cause loss of dorsiflexion, displaying increased ankle joint dorsiflexion when the knee is flexed compared with when it is extended as a positive sign.[9-11]

### Imaging Characteristics

Conventional weight-bearing radiography demonstrates characteristic spurs, which appear as beaklike osseous outgrowths from the anterior margin of the tibial plafond. These can also be accompanied by spurs at the dorsal talar neck (Figure 2). A weight-bearing lateral radiograph with the ankle in maximum dorsiflexion can demonstrate the opposing osseous spurs as seemingly overlapping at the anterior margins of the tibial plafond and talar neck.[12] Although previously described as "kissing osteophytes," morphological analyses with CT have suggested that talar and tibial spurs do not actually impinge upon each other as they are located medial and lateral to the talar dome, respectively.[13] Radiography is usually sufficient to locate and quantify the size of the relative spurs. Talar spur length as determined on plain radiographs correlates positively with talar spur width as measured by CT.[12]

Two grading systems, Anterior Impingement Classification (AIC) and Osteoarthritic Classification (OAC), have been used to assess AIS based on radiography.[14-16]

MRI may also help localize bone spurs.[17] More importantly, however, MRI helps identify intra-articular fibrous bands, which may contribute to impingement, and detect any signs of synovial reactivity such as synovitis, capsular thickening, and formation of scar and granulation tissue (Figures 3, 4).[18-20] Synovial inflammation is optimally seen on fat-suppressed T2 and contrast-enhanced fat-suppressed T1 images as an enhanced signal. MRI can also be useful in excluding other causes of pain that may clinically mimic anterior impingement such as an occult stress fracture of the anterior aspect of the distal tibia or an osteochondral lesion at the medial talar dome.[12]

## Anterolateral Impingement

### Pathophysiology

Anterolateral impingement (ALI) syndrome occurs when there is decreased space in the anterolateral recess—a space bounded by the ATFL and PTFL. A sprain of the ATFL is a common injury that can result in hemarthrosis and subsequent synovitis, contributing to a hyalinized fibroid mass within the recess known as a "meniscoid lesion."[21] Additionally, post-traumatic ligamentous hypertrophy and/or hyperlaxity leads to abnormal contact between the ATFL and osseous structures during movement, altering the normal biomechanics of talus extension into the recess during dorsiflexion.[22,23] Adjacent abnormalities to this recess, such as thickening of the AITFL, the presence of Basset ligament in ankle injury, or spurs at the anterolateral tibia or anterolateral talar neck, can lead to obliteration of the recess.[24-26]

### Physical Exam

Patients typically demonstrate swelling and pain on palpation over the anterolateral joint line; however, most have normal ankle ROM.[27] The anterior impingement test is performed with the patient sitting and the ipsilateral knee bent to 90° while the examiner passively hyperdorsiflexes the affected ankle.


https://doi.org/10.37549/AR-D-24-0064

**Figure 2.** Conventional lateral ankle radiographs demonstrate characteristic spurs at the anterior tibial plafond and talar neck.


**Figure 3.** (A) T1 sagittal image demonstrates osteophytic spurring projecting from the anterior distal tibia and talar neck with surrounding region of soft-tissue fibrosis or focal synovitis. (B) T2 sagittal fat-saturated image demonstrates talar neck and anterior tibial marrow edema-like signal and intra-articular soft-tissue synovitis/fibrosis. (C) T2 coronal fat-saturated image demonstrates intra-articular soft-tissue synovitis/fibrosis.

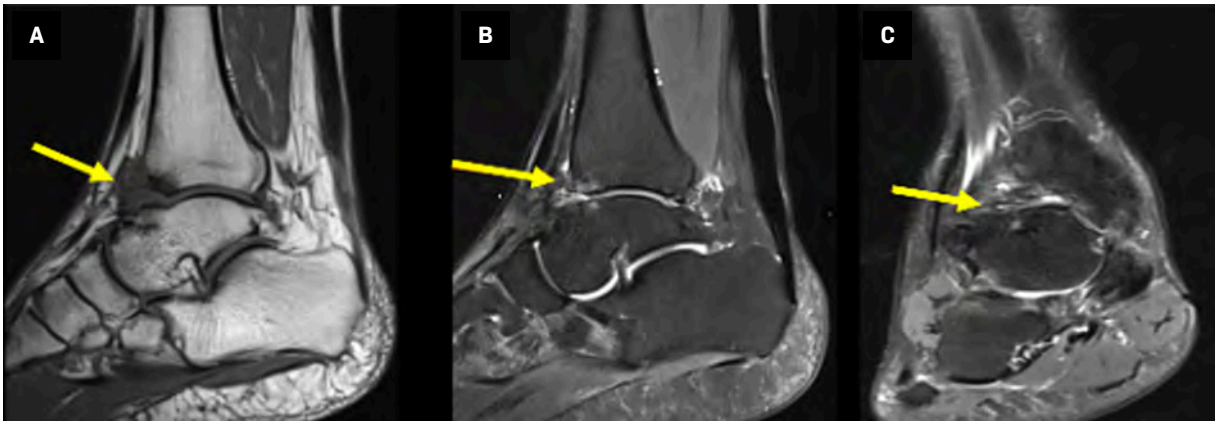


The test is considered positive if pain is elicited over the anterolateral ankle joint line (Figure 5). The anterior drawer test and talar tilt test are also performed to assess integrity of the lateral ligaments and detect possible concomitant instability.

## Imaging Characteristics

Conventional radiography may help identify osteophytes contributing to anterolateral recess obstruction (Figure 6). However, given the etiology of this impingement is primarily related to soft tissue, MRI is often the modality of choice despite its variable sensitivity, which ranges from 42% to 83%.[28] Ligamentous abnormalities such as thickening of ATFL and AITFL, synovial hypertrophy, and scarring in the anterolateral recess may be seen.[28,29] In advanced cases, the fibrotic scar tissue can hyalinize into a meniscoid lesion, which has an intermediate-to-low signal intensity with peripheral rim enhancement on T1 and T2 imaging (Figure 7).[12]

MRI can be used with contrast-enhanced 3D fast spoiled gradient-echo protocols to visualize enhanced vascularized synovial and granulation tissue in the anterolateral recess with sensitivity upward of 91% and accuracy of 87%. These results are comparable to MR arthrography without being as invasive.[30,31] Bone

**Figure 4.** (A) Lateral radiograph of the ankle (top left) demonstrates a large intra-articular body and osteophytic spurring of the anterior talus and anterior distal tibia. (B) T2 fat-saturated sequence sagittal image (top right) demonstrates distal tibial edema-like signal and intra-articular soft-tissue synovitis/fibrosis. (C) T2 fat-saturated sequence axial image (bottom left) demonstrates anterior tibiotalar intra-articular soft-tissue synovitis/fibrosis. (D) T1 sagittal image (bottom right) demonstrates the radiographically large intra-articular body as a hypointense structure (yellow arrow).

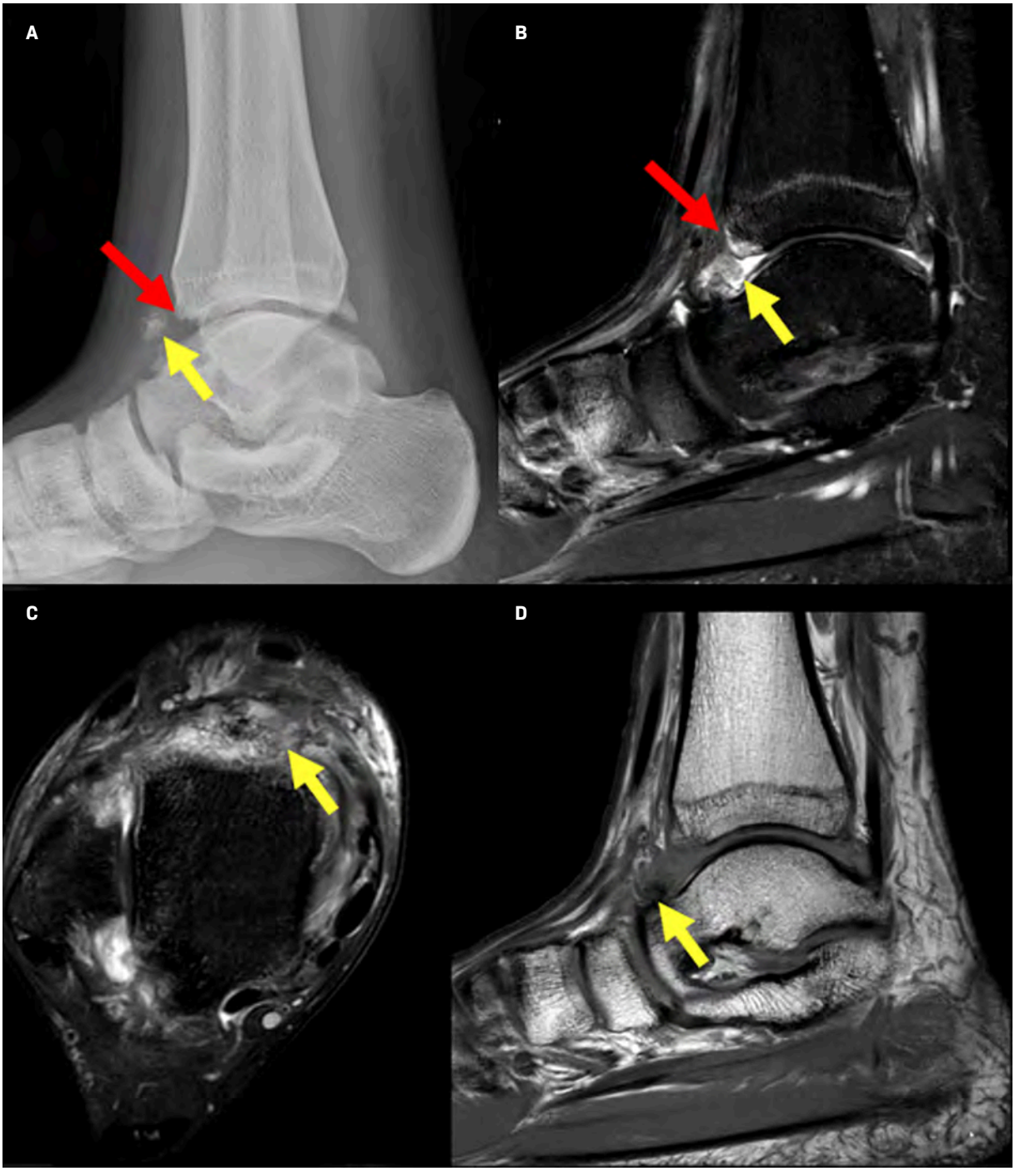




https://doi.org/10.37549/AR-D-24-0064

**Figure 5.** Anterior impingement test demonstrated with passive hyper dorsiflexion to elicit pain in the anterior ankle joint.

**Figure 6.** (A) Sagittal CT image demonstrates osseous spur in the anterior talar neck. (B) Sagittal CT image demonstrates osseous spur in the anterior tibial plafond.


marrow edema is rarely found.[12] It is important to remember that physical exam findings play a particularly crucial role in diagnosing anterolateral ankle impingement. Liu et al demonstrated that physical examination, with a sensitivity and specificity of 94% and 75%, respectively, was more reliable than MRI, at 39% and 50%, for the diagnosis of suspected ALI compared against intra-operative confirmation.[27]

## Anteromedial Impingement

### Pathophysiology

Anteromedial impingement (AMI) has been the focus of little research, owing to its rarity relative to other such syndromes, the strength of the anteromedial joint, and the destabilizing forces required to cause impingement pathologies.[32] Generally, AMI occurs with disruption of the anteromedial recess, which is bounded inferiorly by the ATTL. This can occur in the setting of ATTL thickening or hypertrophic synovial plica resulting from previous trauma or microtrauma, leading to the formation of spurs at the dorsal medial talar neck or anterior aspect of the tibia. Spurs alone are not sufficient for diagnosis.[1,33] Medial malleolar avulsion ossicles (nonunions), common in gymnasts and other athletes in high-stress sports, can also contribute to AMI.[34,35] Nonunion micromotion increases scarring and inflammation, essentially obliterating the medial ankle joint recess between the talus and medial malleolus.

### Physical Exam

Palpation demonstrates pain and swelling over the medial anterior joint line. A forced anterior impingement test may also exacerbate pain, but the test has overall low sensitivity.[34] Important to assess general joint laxity or restriction, ROM testing may also reveal the presence of subtle osteophytes. Ankle valgus stress testing is used to check

**Figure 7.** (A) Axial T1 image and (B) coronal proton density image of the ankle demonstrate scarring in the region of the anterior talofibular ligament with a low-to-intermediate signal meniscoid-shaped mass extending into the lateral ankle gutter.

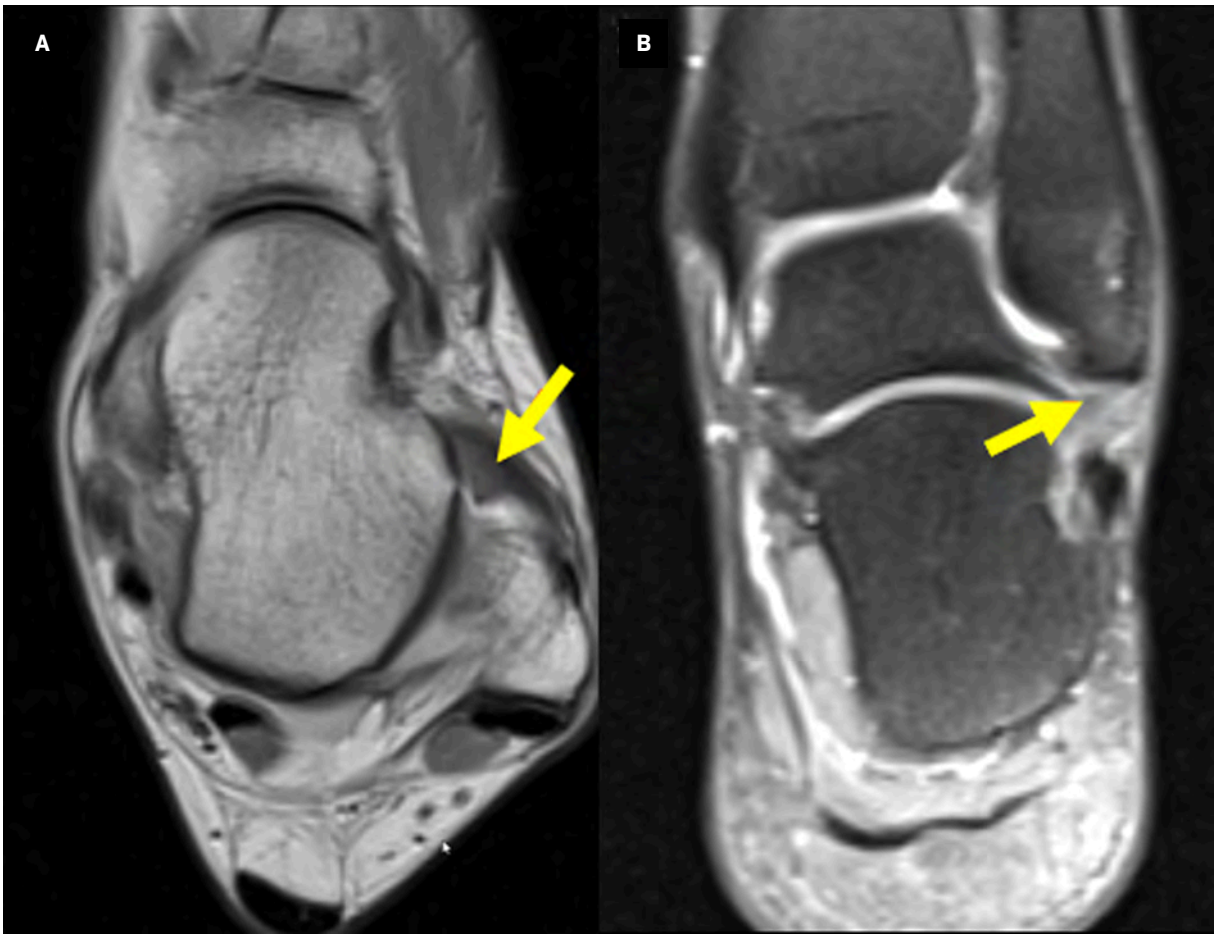


the integrity of the deltoid ligament complex compared with the contralateral ankle; increased laxity or lack of a firm endpoint may indicate more severe injury and instability.

### Imaging Characteristics

Spurs often appear along the most anterior portion of the medial talar facet, along with a corresponding "kissing" osteophyte just anterior to the corner of the medial mortise and the front of the medial malleolus.[36] Anteroposterior and lateral radiographs are limited in diagnostic value because the anteromedial aspect of the tibiotalar joint is concealed by projection of the lateral aspect of the tibia. Instead, a lateral view with a craniocaudal inclination of 45°, with the foot in plantarflexion and the leg rotated 30° externally, is preferred.[14] This nearly doubles the sensitivity for tibial and talar bone spurs (Figure 8).[11]

The role of MRI in detecting AMI has not been established. Images are aimed at visualizing ancillary soft-tissue pathology such as synovitis and deltoid ligament and capsular thickening (Figures 9, 10).[37] The anteromedial recess itself may appear normal.[38] Capsular thickening may be more subtle and can be better detected with intra-articular contrast-enhanced CT or MRI.[37] MRI also plays a role in excluding other abnormalities, such as talar osteochondral injuries, in patients presenting with similar symptoms.

## Posteromedial Impingement

### Pathophysiology

Posteromedial impingement (PMI) is often related to damage to the PTTL, which lies anterior to the posteromedial recess. Swelling from hypertrophy caused by healing of the PTTL can lead to entrapment of the posteromedial tibiotalar joint capsule.[39] One arthroscopic study


https://doi.org/10.37549/AR-D-24-0064

**Figure 8.** Anteroposterior radiograph of the ankle demonstrates medial malleolar bone spur formation.

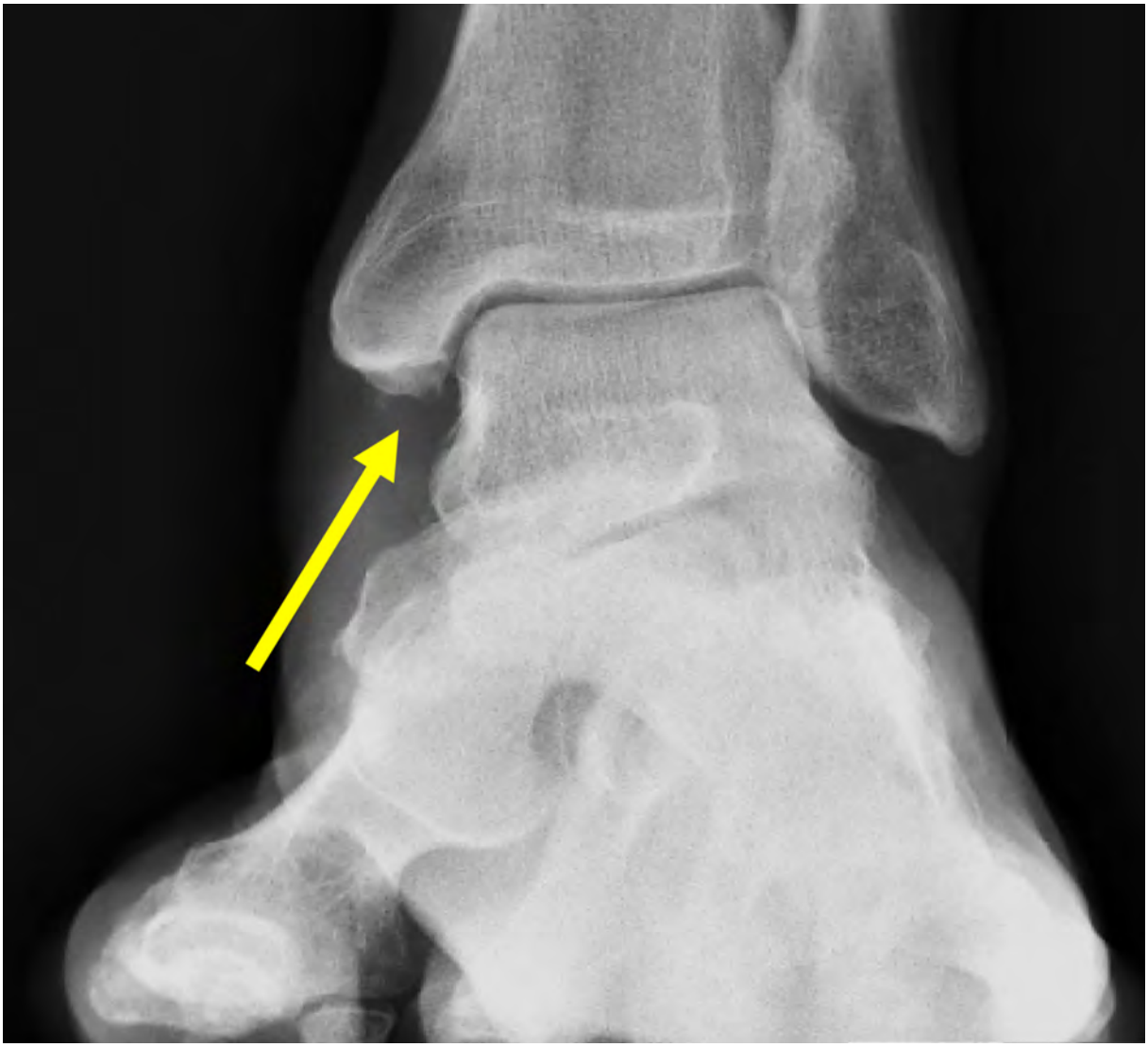

found concurrent distal medial malleolus and talar facet articular cartilage injuries in affected patients, indicating a possible association.[40]

### Physical Exam

Clinical history and radiography are more useful in diagnosing PMI, owing to the challenges in examining the deeper posterior ankle tendons and ligaments.[41,42] Posteromedial pressure during ankle inversion and plantarflexion enhances identifying pain in the posteromedial corner; gait analysis is also useful as it can help differentiate true posterior tibial tendon dysfunction from PMI, which is associated with entrapment of the PTTL portion of the deltoid ligament.[43]

### Imaging Characteristics

As pathophysiology is largely related to soft-tissue pathology, radiography plays a little role in imaging for PMI syndromes. Radiographs may show periosteal new bone formation along the posteromedial wall of the talus and along the medial malleolus.[43] On MRI, signs can vary based on chronicity; in the subacute stage (within 4 weeks post-injury), the primary finding can be increased signal in the posteromedial capsule and the PTFL, whereas chronic stages (greater than 14 weeks post-injury) demonstrate a higher incidence of PTTL disruption with thickening and loss of normal fibrillar pattern, resulting in an amorphous appearance (Figure 11).[42] Fluid-sensitive sequences increase the conspicuity of synovitis, which may be seen as a focal increased signal relative to adjacent tissue.[44] Marrow

**Figure 9.** (A, B) Axial proton density and proton density fat-saturated images demonstrate thickening and increased signal intensity of anteromedial ankle soft tissues, including the tibial spring ligament and the superficial portion of the deltoid ligament. Note that the tibialis posterior tendon (green arrow) demonstrates a normal appearance, arguing against a sequela of posterior tibial tendon dysfunction. (C) Coronal proton density fat-saturated image demonstrates thickening and edema of the anteromedial ankle soft tissues.

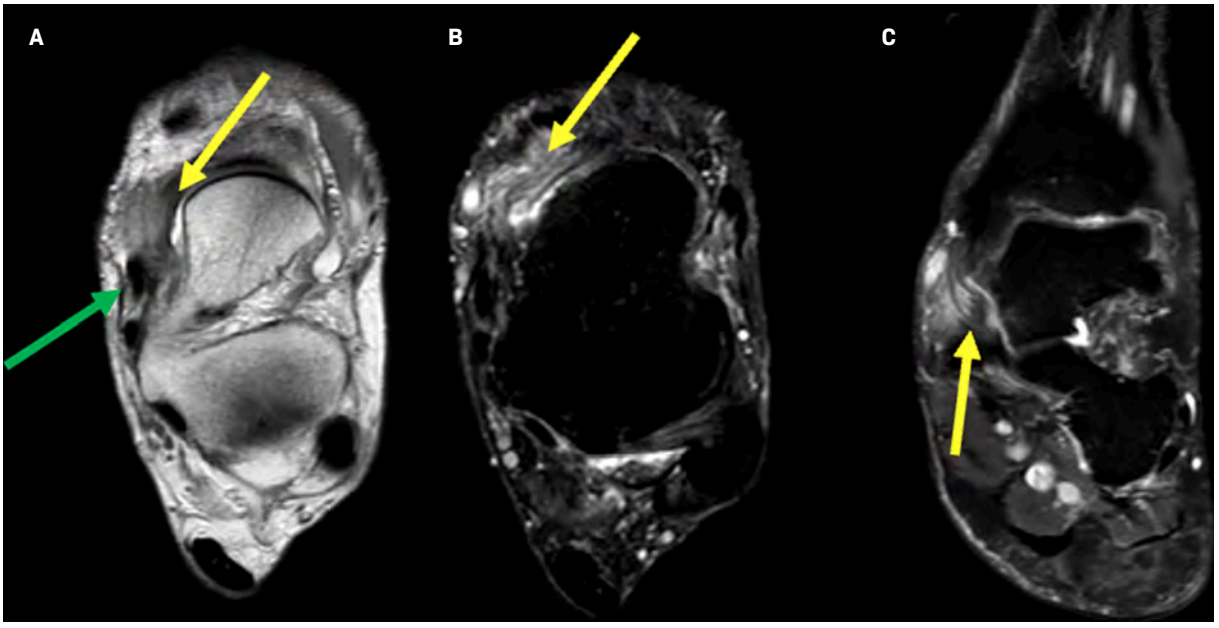


**Figure 10.** (A) Anteroposterior radiograph of the foot shows osteophytic spurring of the medial talar neck and the distal tip of the medial malleolus. (B) Axial T2 fat-saturated image of the ankle demonstrates a reactive marrow edema-like signal of the medial talus and focal synovitis in the anteromedial gutter. (C) Coronal proton density fat-saturated image of the ankle demonstrates thickening of the deltoid ligament, focal synovitis in the anteromedial gutter, and reactive marrow edema-like signal of the talus.

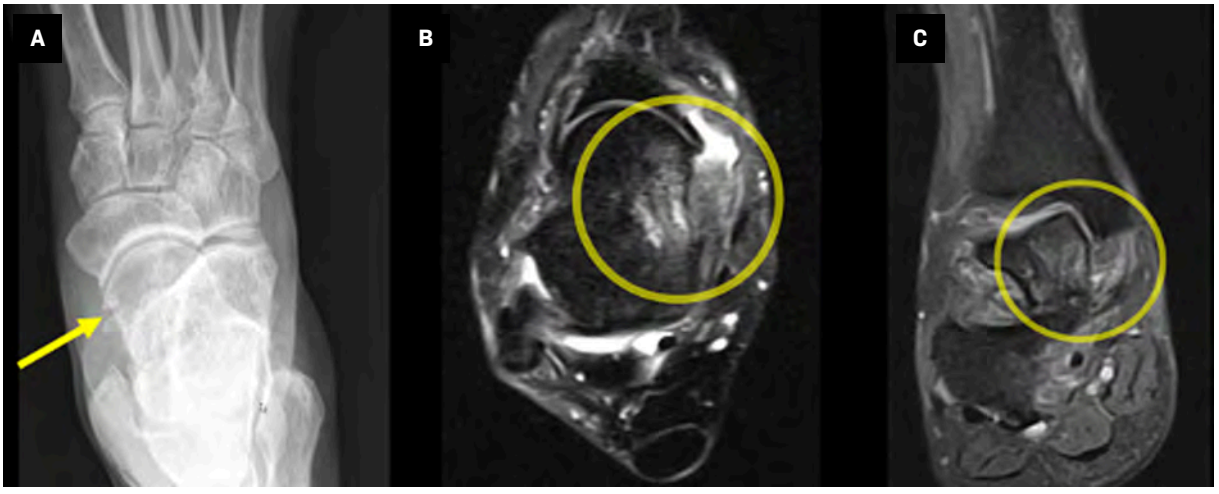


edema can be seen infrequently and has no specific distribution.[45] In general, bone changes are less common in PMI; however, small cortical avulsion fractures may be present in the PTTL and are best demonstrated on CT.[44]

## Posterior Impingement

### Pathophysiology

The posterior ankle is bordered by the posterior tibia and calcaneus and extends to the Kager fat pad. Compression within this region during plantar flexion is characteristic of posterior impingement (PI) syndrome.

In particular, os trigonum is a common finding, seen in up to 63% of patients with PI.[46] Normally, the


https://doi.org/10.37549/AR-D-24-0064

**Figure 11.** (A) Coronal T2 fat-saturated image of the ankle demonstrates reactive edema-like signal and fluid within the posteriomedial ankle, likely owing to impingement by prominent talocalcaneal osteophytes. (B) Axial T2 fat-saturated image of the ankle demonstrates thickening and loss of the normal deltoid ligament striations and marked posteromedial soft-tissue swelling.

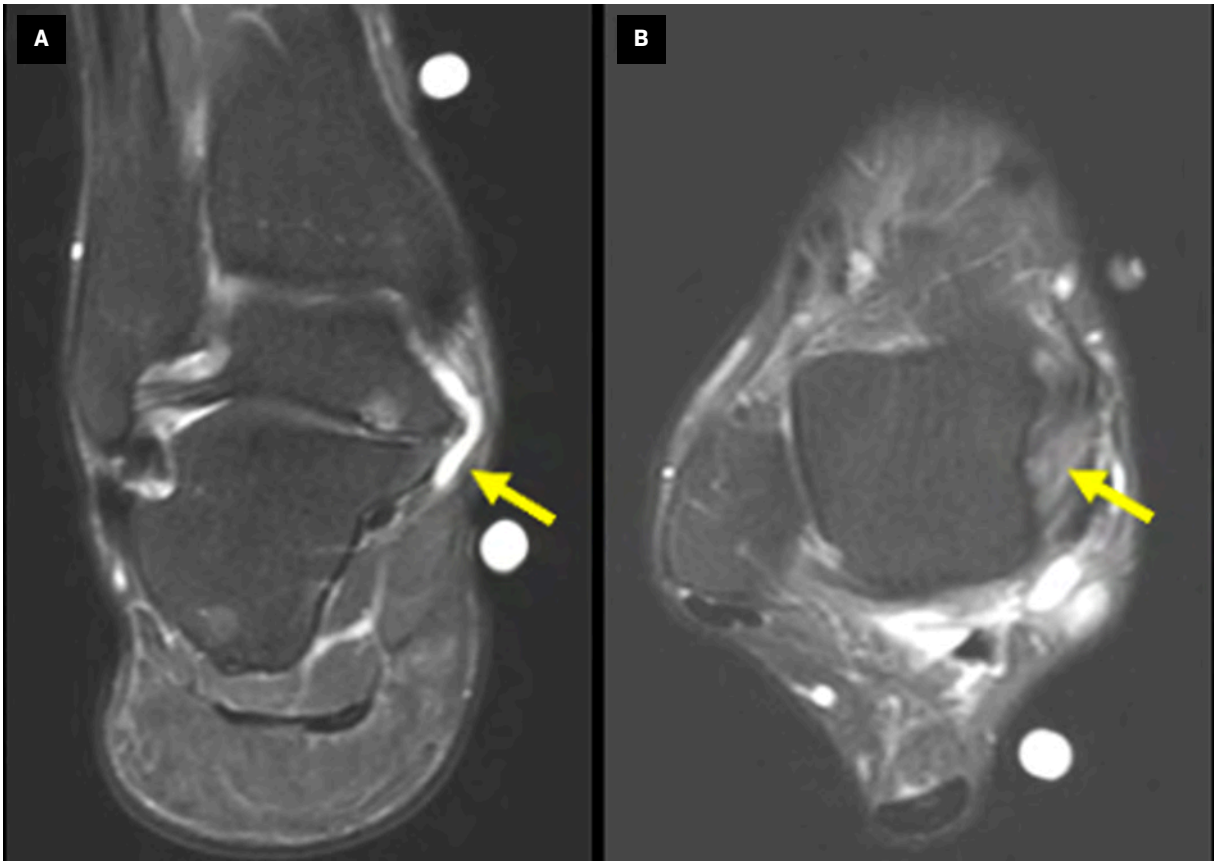


Weight-bearing radiography in the anteroposterior, latera.

secondary ossification center of the posterolateral talus forms between the ages of 8 and 13 years and fuses within 1 year; however, 7 % of the time a lack of fusion can result in an os trigonum.[47] Other osseous pathologies, such as chronic fracture nonunion of the medial tubercle of the posterior talus, can present with a similar clinical picture or a congenital Stieda process, which is a fusion of a secondary ossification center, resulting in posterolateral elongation of the talus.[46]

## Physical Exam

Examination involves passive hyperplantarflexion of the ankle while using 2 fingers to palpate just lateral to the Achilles tendon at the level of the distal fibula; PI is suspected if the patient's pain is reproduced. Contributing pathology can be delineated with maneuvers such as the Tomassen test, in which a positive result reveals decreased ROM of the great toe metatarsophalangeal joint with the ankle dorsiflexed. This can suggest FHL pathology (Figure 12). Additional maneuvers, such as a calcaneal squeeze test, which involves squeezing both sides of the posterior tuberosity, can raise concern for differential diagnoses such as a calcaneal stress fracture involving the posterior tuberosity.

## Imaging Characteristics

Weight-bearing radiography in the anteroposterior, lateral, and mortise views, along with an oblique view of the foot, is important for treatment planning. The oblique view, with the foot in 25° of external rotation, can help differentiate hypertrophy of the posterior talar process from os trigonum in cases of bony impingement.[48] Advanced imaging may also be necessary in equivocal cases.

Os trigonum in the lateral view is the most pertinent radiographic finding when assessing for PI; however, its presence

**Figure 12.** Normal examination of great toe metatarsophalangeal joint pathology range of motion, which is greater in ankle plantarflexion than ankle dorsiflexion. Alternative findings can be suggestive of flexor hallucis longus pathology.

**Figure 13.** (A) Axial T2 fat-saturated image demonstrates thickening of the posterior talofibular ligament. (B) Axial T2 fat-saturated image demonstrates thickening of the posterior intermalleolar ligament. (C) Sagittal T2 fat-saturated image demonstrates abnormal edema adjacent to the posterior talus suggestive of posterior ankle impingement. (D) Sagittal T1 image demonstrates a prominent os trigonum.

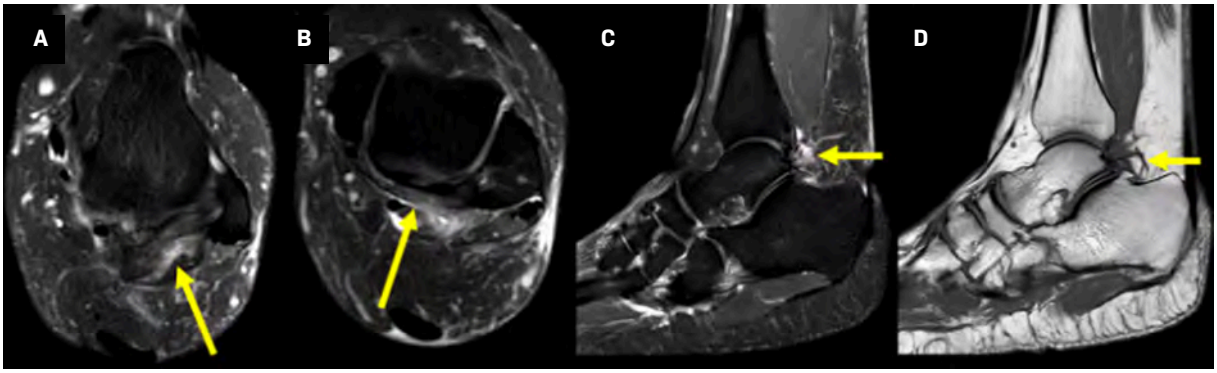


alone is not sufficient to cause impingement, but it can contribute to symptomatology.[18] Up to 14% of the asymptomatic population may have an os trigonum.[49]

CT facilitates the assessment of osseous changes between the os trigonum and talus, such as fragmentation of the os and pressure-related erosions along the talus.[49] On MRI, PI can present with bone marrow edema within the talus, os trigonum, increased signal at synchondrosis, fluid accumulation around the posterior talus and tibia, and synovitis with thickening of posterior ligaments (Figures 13, 14).[50] In certain populations such as ballet dancers, who frequently practice maximal plantar flexion, hyaline-like cartilage can form on the posterior talus, appearing as low-signal intensity on T2 images.[51]

## Treatment

Despite mixed study findings in the literature, standard initial therapy of AISs consists of nonsteroidal anti-inflammatory drugs, physical therapy, and intra-articular steroid injections for 3-6 months to reduce stress on the joint and promote healing.[8,9,11,52]

Surgical intervention may be warranted if pain or restriction persists beyond 6 months. Surgery aims to remove osteophytes, debride inflamed soft tissue and loose fragments in the joint space, and correct coexisting contributing conditions.[6-8,11,15,22,,34] While open arthrotomy was once considered the standard procedure, complications such as cutaneous nerve entrapment, long extensor tendon damage, wound dehiscence, and hypertrophic scar tissue formation led to a shift toward arthroscopy, reducing recovery times and complication rates (Figures 15–19).[6,11,16,53-55]

## Conclusion

Imaging plays an important role in localizing pathology and guiding treatment of AISs. Choice of modality is based largely on the pathophysiology of the impingement.

Radiography is particularly useful in cases caused by ossesous abnormalities such as AI. As mentioned earlier, 2 commonly


https://doi.org/10.37549/AR-D-24-0064

**Figure 14.** (A) Lateral radiograph of the ankle demonstrates an os trigonum. (B) Axial T2 fat-saturated image shows reactive marrow edema-like signal of the os trigonum, fluid across the synchondrosis, and marked posterior synovitis. (C) Sagittal T2 image shows reactive marrow edema-like signal of the talus and os trigonum with reactive posterior tibiotalar and subtalar joint effusions.

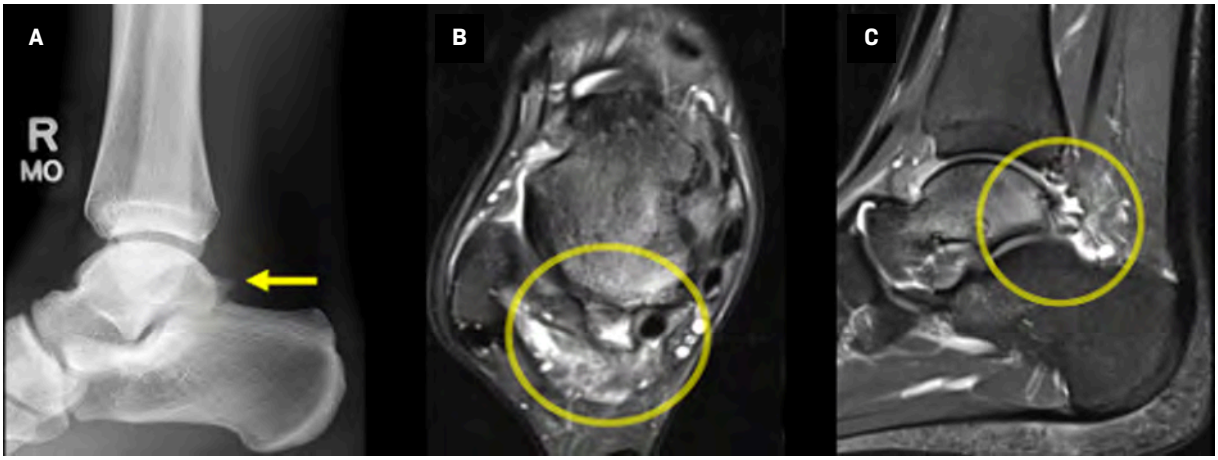


**Figure 15.** Surgical management of anterior impingement. (A) Anterolateral arthroscopic view shows talar spur, with arrows pointing at approximate demarcation from the talus neck and shaver burr holding up the joint capsule. (B) Medial arthroscopic view after debridement with arrows demonstrates a restoration of the concavity of the talar neck with restoration of normal anatomic profile.

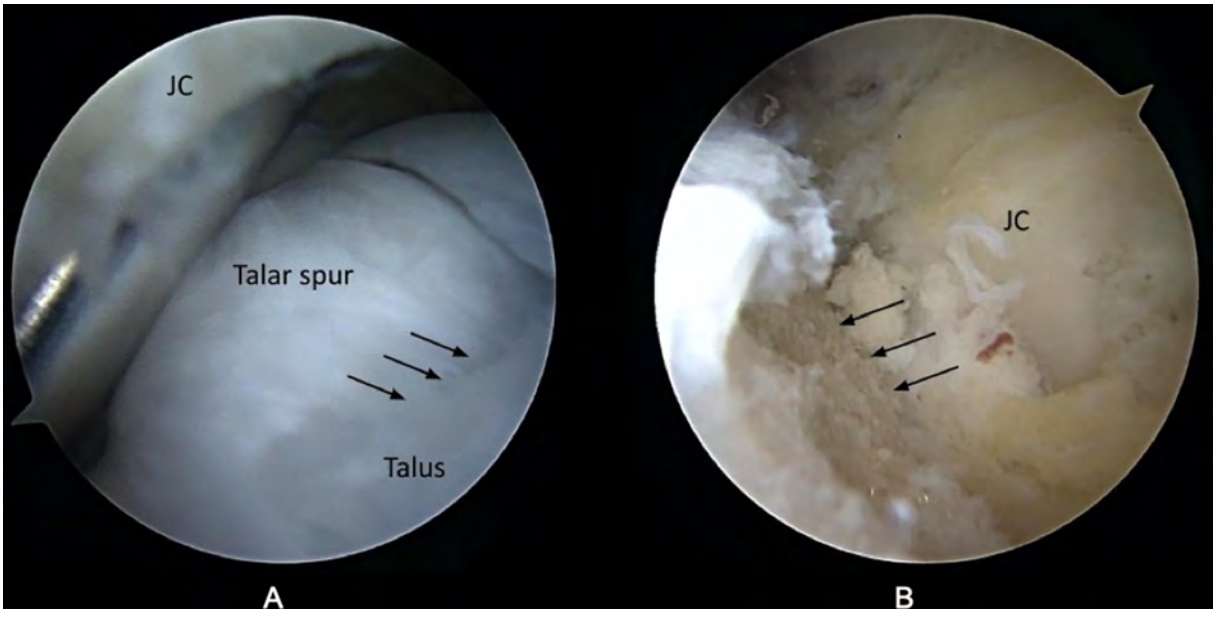


used classification systems for AI are the AIC and OAC. Preoperative staging, especially regarding the extent of degenerative changes, is a significant factor in predicting treatment outcomes in anterior impingement types. When using AIC, arthroscopic surgical interventions have demonstrated good outcomes in type I and II AI, with less successful outcomes in type III and IV cases.[19,20] The OAC can also be predictive of outcomes; arthroscopic surgical interventions have been reported to deliver good outcomes in patients with grade O/I impingements, while not faring as well in patients with grade II/III impingments.[19,53] Van Dijk et al found that the OAC classification was a better predictor of surgical outcomesl[19]; however, Coull et al concluded that the OAC system did not provide enough detail and that patients were too broadly grouped.[14] Further studies comparing the 2 classification systems as well as developing additional systems for other impingement syndromes would be useful in quantifying image findings for surgical planning.

In some cases, CT can permit a more detailed assessment of the

**Figure 16.** Surgical management of anterior impingement. (A) Anterolateral arthroscopic view of relative anatomy shows a loose body encased in arthrofibrotic bands with the tibia seen behind. (B) Central arthroscopic view of deformation after the loose body and arthrofibrotic band were debrided showing chondromalacia on the tibia.

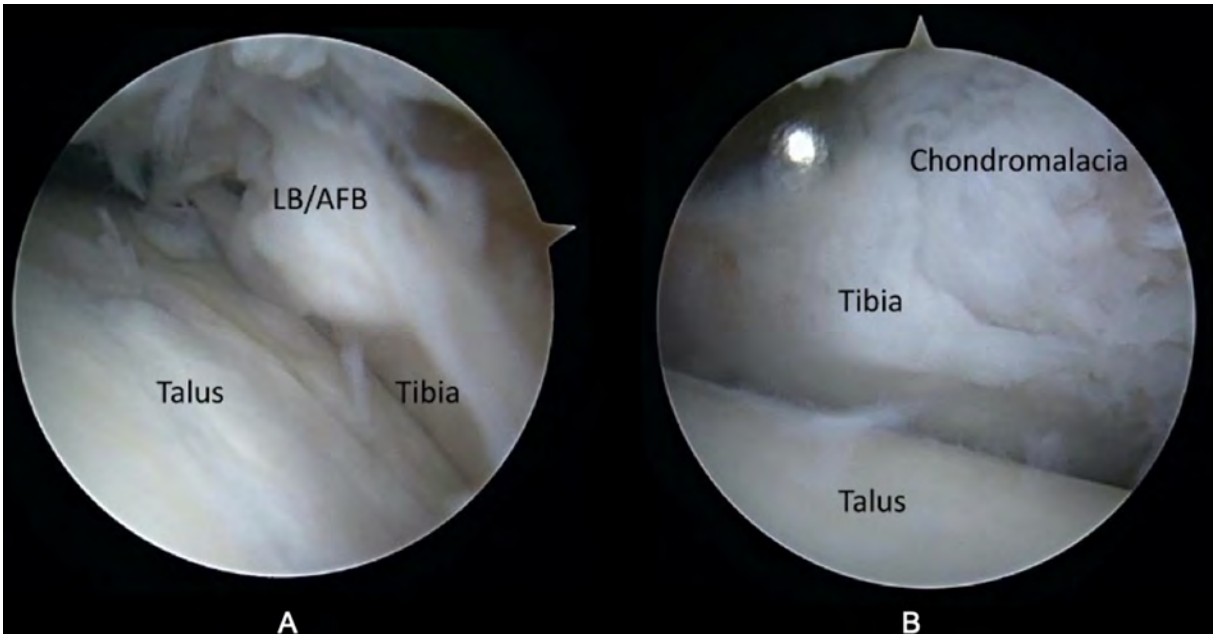


**Figure 17.** : Surgical management of anterolateral impingement. (A) Anterolateral arthroscopic view with meniscoid lesion in syndesmosis. (B) Arthroscopic view of anatomy after debridement of syndesmotic meniscoid lesion.

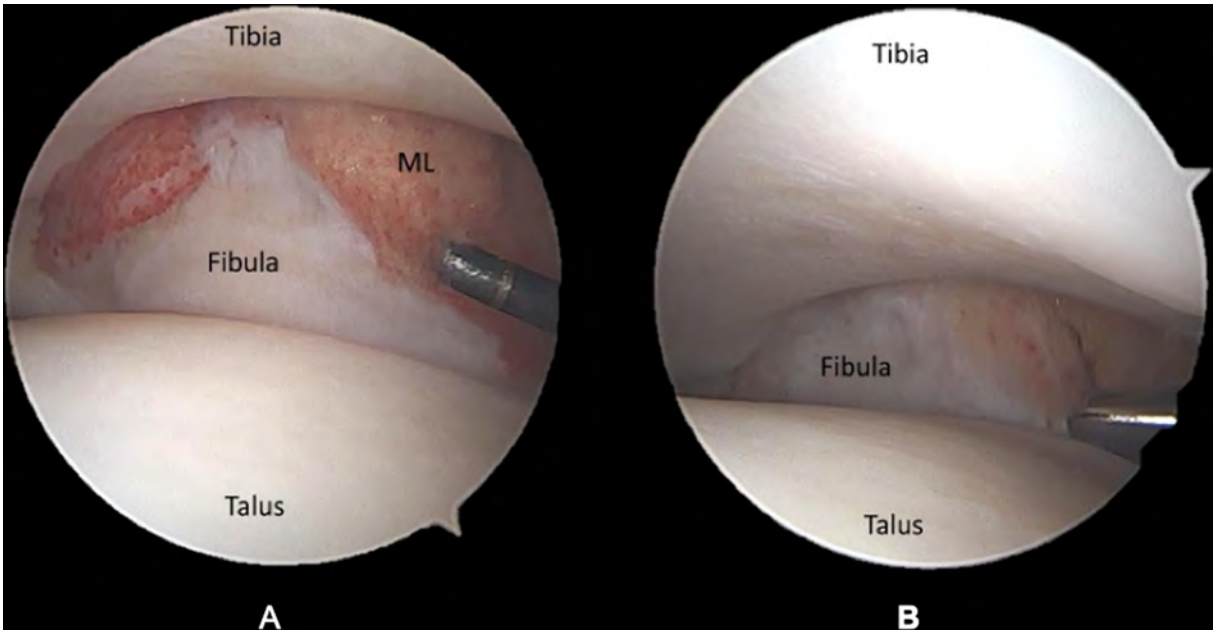



https://doi.org/10.37549/AR-D-24-0064

**Figure 18.** Surgical management of anteromedial impingement. (A) Arthroscopic view of hypertrophied anteromedial plica band. (B) Arthroscopic view after the removal of plica band and debridement shows medial malleolus and restoration of relative anatomy.

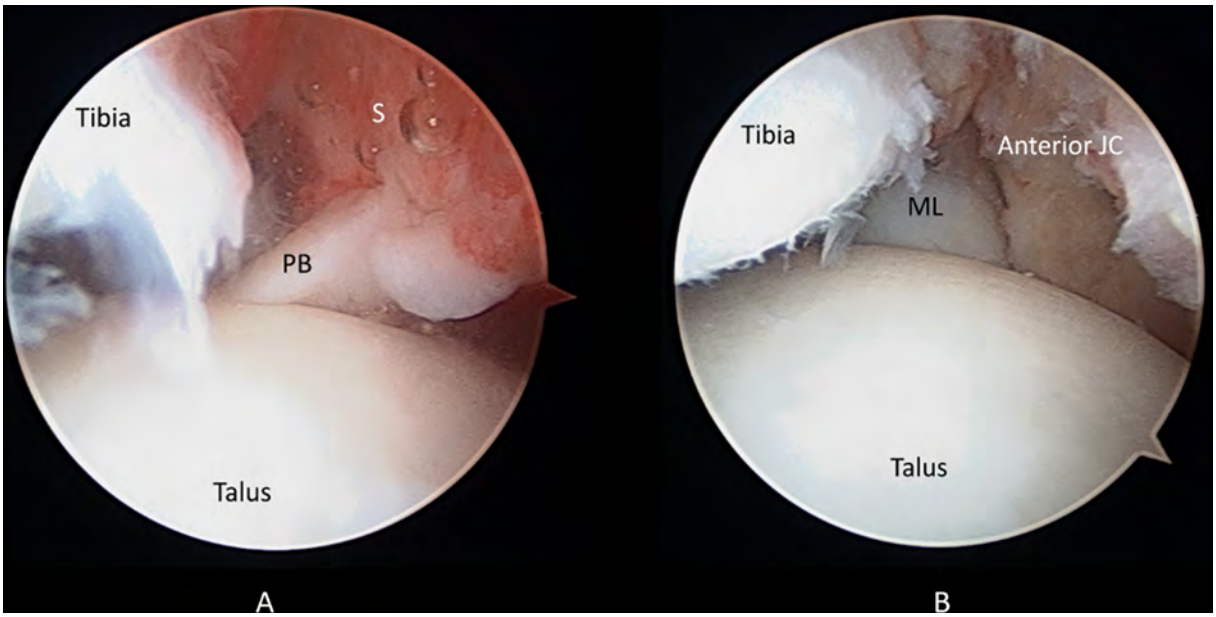


**Figure 19.** Surgical management of posterior impingement. (A) Relative osseus anatomy demonstrates os trigonum, calcaneus, and talus. (B) Hindfoot endoscopy view shows complete os trigonum removal after resection of medial and lateral attachments.

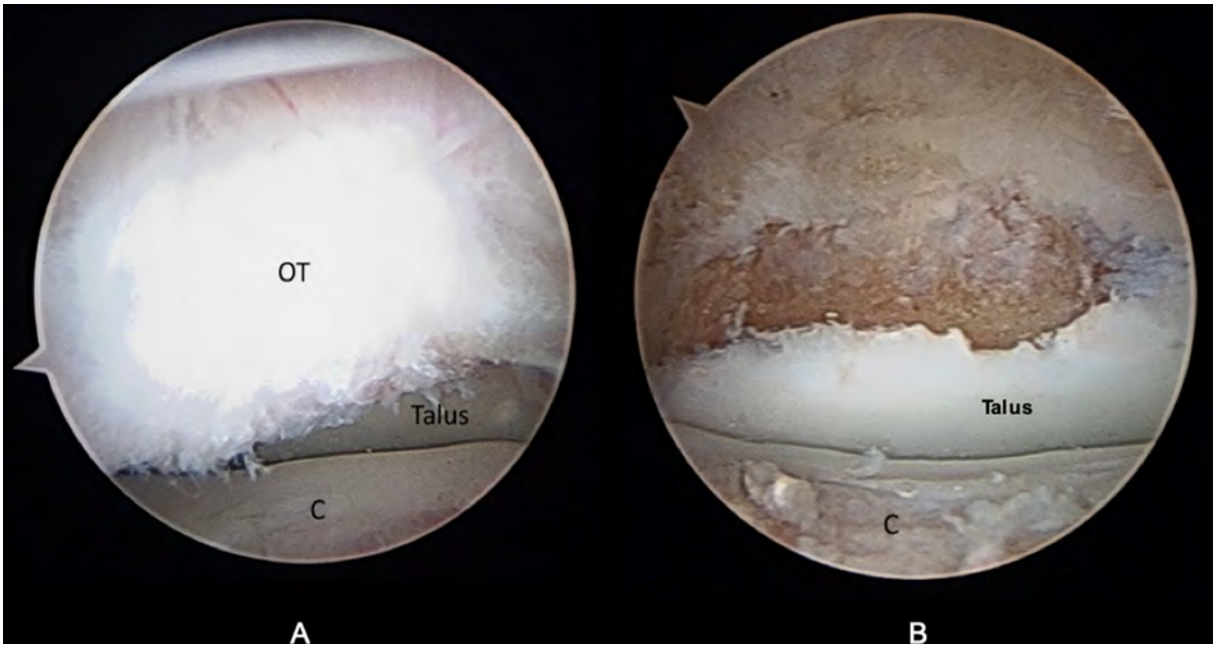

location and burden of osteophytes and other osseous abnormalities, particularly in cases where the physical exam and history are not consistent with initial imaging findings. Indeed, more detailed imaging can sometimes change the diagnosis from a single form of impingement to a combined type, potentially redirecting the approach to treatment.[56]

As CT provides limited information on bone marrow and soft-tissue abnormalities, MRI can be useful in syndromes caused predominantly by soft-tissue pathology. Alternatively, patients without clinical symptoms or signs of AIS have been found to have incidental abnormalities on MR arthrography that are then confirmed at surgery.[57] Thus, a thorough history and physical examination are important to accurately correlate imaging features and treat only symptomatic cases of AISs.

## References

1) Glenzer SR, Domingue GA, Perry MD. Anteromedial ankle impingement due to a talar cam lesion and anterior deep deltoid ligament with variant anatomy: a case report. *Foot Ankle Orthop*. 2020;5(4). doi:10.1177/2473011420977427

2) Yang Q, Zhou Y, Xu Y. Arthroscopic debridement of anterior ankle impingement in patients with chronic lateral ankle instability. *BMC Musculoskelet Disord*. 2018;19(1):239. doi:10.1186/s12891-018-2168-6

3) Mosca M, Caravelli S, Fuiano M, et al. Management of early ankle osteoarthritis through anterior joint-preserving surgery: a retrospective evaluation at mid- to long-term follow-up. *Eur J Orthop Surg Traumatol*. 2020;30(7):1171-1178. doi:10.1007/s00590-020-02691-6

4) Viehöfer AF, Casari F, Waibel FWA, et al. Smoking is associated with anterior ankle impingement after isolated autologous matrix-induced chondrogenesis for osteochondral lesions of the talus. *Cartilage*. 2021;13(1_suppl):1366S-1372S. doi:10.1177/1947603520959405

5) Morelli F, Princi G, Rossato A, Iorio R, Ferretti A. Pigmented villonodular synovitis: a rare case of anterior ankle impingement. *J Orthop Case Rep*. 2019;10(1):16-18. doi:10.13107/jocr.2019.v10.i01.1618

6) Hawkins RB. Arthroscopic treatment of sports-related anterior osteophytes in the ankle. *Foot Ankle*. 1988;9(2):87-90. doi:10.1177/107110078800900205

7) McMurray TP. Footballer's ankle. *J Bone Joint Surg Br*. 1950;32-B(1):68-69. doi:10.1302/0301-620X.32B1.68

8) Talusan PG, Toy J, Perez JL, Milewski MD, Reach JS Jr. Anterior ankle impingement: diagnosis and treatment. *J Am Acad Orthop Surg*. 2014;22(5):333-339. doi:10.5435/JAAOS-22-05-333

9) Branca A, Di Palma L, Bucca C, Visconti CS, Di Mille M. Arthroscopic treatment of anterior ankle impingement. *Foot Ankle Int*. 1997;18(7):418-423. doi:10.1177/107110079701800708

10) Sanders TG, Rathur SK. Impingement syndromes of the ankle. *Magn Reson Imaging Clin N Am*. 2008;16(1):29-38. doi:10.1016/j.mric.2008.02.005

11) Tol JL, van Dijk CN. Anterior ankle impingement. *Foot Ankle Clin*. 2006;11(2):297-310. doi:10.1016/j.fcl.2006.02.002

12) Al-Riyami AM, Tan HK, Peh WCG. Imaging of ankle impingement syndromes. *Can Assoc Radiol J*. 2017;68(4):431-437. doi:10.1016/j.carj.2017.04.001

13) Berberian WS, Hecht PJ, Wapner KL, DiVerniero R. Morphology of tibiotalar osteophytes in anterior ankle impingement. *Foot Ankle Int*. 2001;22(4):313-317. doi:10.1177/107110070102200407

14) van Dijk CN, Tol JL, Verheyen CC. A prospective study of prognostic factors concerning the outcome of arthroscopic surgery for anterior ankle impingement. *Am J Sports Med*. 1997;25(6):737-745. doi:10.1177/036354659702500603

15) Scranton PE Jr, McDermott JE. Anterior tibiotalar spurs: a comparison of open versus arthroscopic debridement. *Foot Ankle*. 1992;13(3):125-129. doi:10.1177/107110079201300303

16) Coull R, Raffiq T, James LE, Stephens MM. Open treatment of anterior impingement of the ankle. *J Bone Joint Surg Br*. 2003;85(4):550-553. doi:10.1302/0301-620x.85b4.13871

17) Shim DW, Kim S, Hwang Y, et al. Detection of the tram track lesion in the ankle joint: comparing 3.0-tesla magnetic resonance imaging and arthroscopy. *Arthroscopy*. 2018;34(3):866-871. doi:10.1016/j.arthro.2017.09.014

18) Berman Z, Tafur M, Ahmed SS, Huang BK, Chang EY. Ankle impingement syndromes: an imaging review. *Br J Radiol*. 2017;90(1070):20160735. doi:10.1259/bjr.20160735

19) Haller J, Bernt R, Seeger T, et al. MR-imaging of anterior tibiotalar impingement syndrome: agreement, sensitivity and specificity of MR-imaging and indirect MR-arthrography. *Eur J Radiol*. 2006;58(3):450-460. doi:10.1016/j.ejrad.2006.03.008

20) Zbojniewicz AM. Impingement syndromes of the ankle and hindfoot. *Pediatr Radiol*. 2019;49(12):1691-1701. doi:10.1007/s00247-019-04459-5

21) Wolin I, Gassmani F, Sheinman S, Levinthal DH. Internal derangement of the talofibular component of the ankle. *Surg Gynecol Obstet*. 1950;91(2):193-200.

22) Bassett FH 3rd, Gates HS 3rd, Billys JB, Morris HB, Nikolaou PK. Talar impingement by the anteroinferior tibiofibular ligament. A cause of chronic pain in the ankle after inversion sprain. *J Bone Joint Surg*. 1990;72(1):55-59. doi:10.2106/00004623-199072010-00009

23) van den Bekerom MPJ, Raven EEJ. The distal fascicle of the anterior inferior tibiofibular ligament as a cause of tibiotalar impingement syndrome: a current concepts review. *Knee Surg Sports Traumatol Arthrosc*. 2007;15(4):465-471. doi:10.1007/s00167-006-0275-7

24) Odak S, Ahluwalia R, Shivarathre DG, et al. Arthroscopic evaluation of impingement and osteochondral lesions in chronic lateral ankle instability. *Foot Ankle Int*. 2015;36(9):1045-1049. doi:10.1177/1071100715585525

25) Talbot CE, Knapik DM, Miskovsky SN. Prevalence and location of bone spurs in anterior ankle impingement: a cadaveric investigation. *Clin Anat*. 2018;31(8):1144-1150. doi:10.1002/ca.23216

26) Edama M, Kageyama I, Kikumoto T, et al. Morphological features of the anterior talofibular ligament by the number of fiber bundles. *Ann Anat*. 2018;216:69-74. doi:10.1016/j.aanat.2017.11.001

27) Liu SH, Raskin A, Osti L, et al. Arthroscopic treatment of anterolateral ankle impingement. *Arthroscopy*. 1994;10(2):215-218. doi:10.1016/S0749-8063(05)80097-0

28) Duncan D, Mologne T, Hildebrand H, et al. The usefulness of magnetic resonance imaging in the diagnosis of anterolateral impingement of the ankle. *J Foot Ankle Surg*. 2006;45(5):304-307. doi:10.1053/j.jfas.2006.06.003

29) De Maeseneer M, Wuertzer S, de Mey J, Shahabpour M. The imaging findings of impingement syndromes of the lower limb. *Clin Radiol*. 2017;72(12):1014-1024. doi:10.1016/j.crad.2017.07.018

30) Choo HJ, Suh J-S, Kim S-J, et al. Ankle MRI for anterolateral soft tissue impingement: increased accuracy with the use of contrast-enhanced fat-suppressed 3D-FSPGR MRI. *Korean J Radiol*. 2008;9(5):409-415. doi:10.3348/kjr.2008.9.5.409

31) Lee JW, Suh JS, Huh YM, Moon ES, Kim SJ. Soft tissue impingement syndrome of the ankle: diagnostic efficacy of MRI and clinical results after arthroscopic treatment. *Foot Ankle Int*. 2004;25(12):896-902. doi:10.1177/107110070402501209

32) Shane AM, Reeves CL, Vazales R, Farley Z. Soft tissue impingement of the ankle: pathophysiology, evaluation, and arthroscopic treatment. *Clin Podiatr Med Surg*. 2016;33(4):503-520. doi:10.1016/j.cpm.2016.06.003

33) Massada JL. Ankle overuse injuries in soccer players. morphological adaptation of the talus in the anterior impingement. *J Sports Med Phys Fitness*. 1991;31(3):447-451.

34) Ross KA, Murawski CD, Smyth NA, et al. Current concepts review: arthroscopic treatment of anterior ankle impingement. *Foot Ankle Surg*. 2017;23(1):1-8. doi:10.1016/j.fas.2016.01.005

35) Vann MA II, Manoli A II. Medial ankle impingement syndrome in female gymnasts. *Oper Tech Sports Med*. 2010;18(1):50-52. doi:10.1053/j.otsm.2009.11.003



https://doi.org/10.37549/AR-D-24-0064

36) Russo A, Zappia M, Reginelli A, et al. Ankle impingement: a review of multimodality imaging approach. *Musculoskelet Surg*. 2013;97 Suppl 2:S161-8. doi:10.1007/s12306-013-0286-8

37) Donovan A, Rosenberg ZS. MRI of ankle and lateral hindfoot impingement syndromes. *AJR Am J Roentgenol*. 2010;195(3):595-604. doi:10.2214/AJR.09.4199

38) Robinson P, White LM, Salonen D, Ogilvie-Harris D. Anteromedial impingement of the ankle: using MR arthrography to assess the anteromedial recess. *Am J Roentgenol*. 2002;178(3):601-604. doi:10.2214/ajr.178.3.1780601

39) Song W, Liu W, Chen B, et al. Posteromedial ankle impingement caused by hypertrophy of talocalcaneal coalition: a report of five cases and introduction of a novel index system. *J Foot Ankle Surg*. 2016;55(6):1312-1317. doi:10.1053/j.jfas.2016.01.005

40) van Dijk CN, Wessel RN, Tol JL, Maas M. Oblique radiograph for the detection of bone spurs in anterior ankle impingement. *Skeletal Radiol*. 2002;31(4):214-221. doi:10.1007/s00256-002-0477-0

41) Giannini S, Buda R, Mosca M, Parma A, Di Caprio F. Posterior ankle impingement. *Foot Ankle Int*. 2013;34(3):459-465. doi:10.1177/1071100713477609

42) Koulouris G, Connell D, Schneider T, Edwards W. Posterior tibiotalar ligament injury resulting in posteromedial impingement. *Foot Ankle Int*. 2003;24(8):575-583. doi:10.1177/107110070302400802

43) Paterson RS, Brown JN. The posteromedial impingement lesion of the ankle. A series of six cases. *Am J Sports Med*. 2001;29(5):550-557. doi:10.1177/03635465010290050501

44) LiMarzi GM, Scherer KF, Richardson ML, et al. CT and mr imaging of the postoperative ankle and foot. *Radiographics*. 2016;36(6):1828-1848. doi:10.1148/rg.2016160016

45) Messiou C, Robinson P, O'Connor PJ, Grainger A. Subacute posteromedial impingement of the ankle in athletes: MR imaging evaluation and ultrasound guided therapy. *Skeletal Radiol*. 2006;35(2):88-94. doi:10.1007/s00256-005-0049-1

46) Srirangarajan T, Abbasian A. Chronic fracture of the posteromedial tubercle of the talus masquerading as os trigonum syndrome. *Case Rep Orthop*. 2021;2021:6637081. doi:10.1155/2021/6637081

47) Özer M, Yıldırım A. Evaluation of the prevalence of os trigonum and talus osteochondral lesions in ankle magnetic resonance imaging of patients with ankle impingement syndrome. *J Foot Ankle Surg*. 2019;58(2):273-277. doi:10.1053/j.jfas.2018.08.043

48) Gasparetto F, Collo G, Pisanu G, et al. Posterior ankle and subtalar arthroscopy: indications, technique, and results. *Curr Rev Musculoskelet Med*. 2012;5(2):164-170. doi:10.1007/s12178-012-9118-y

49) Karasick D, Schweitzer ME. The os trigonum syndrome: imaging features. *AJR Am J Roentgenol*. 1996;166(1):125-129. doi:10.2214/ajr.166.1.8571860

50) Bureau NJ, Cardinal E, Hobden R, Aubin B. Posterior ankle impingement syndrome: MR imaging findings in seven patients. *Radiology*. 2000;215(2):497-503. doi:10.1148/radiology.215.2.r00ma01497

51) Kinugasa K, Shimomura K, Tachibana Y, et al. Posterior ankle impingement caused by hyaline-like cartilage generation in ballet dancers-a report of 2 cases. *J Foot Ankle Surg*. 2022;61(4):e9-e14. doi:10.1053/j.jfas.2021.10.015

52) Ogilvie-Harris DJ, Mahomed N, Demazière A. Anterior impingement of the ankle treated by arthroscopic removal of bony spurs. *J Bone Joint Surg Br*. 1993;75(3):437-440. doi:10.1302/0301-620X.75B3.8496216

53) Martin DF, Baker CL, Curl WW, et al. Operative ankle arthroscopy. *Am J Sports Med*. 1989;17(1):16-23. doi:10.1177/036354658901700103

54) O'Donoghue DH. Impingement exostoses of the talus and tibia. *J Bone Joint Surg Am*. 1957;39-A(4):835-852.

55) Parkes JC II, Hamilton WG, Patterson AH, Rawles JG. The anterior impingement syndrome of the ankle. *J Trauma*. 1980;20(10):895-898. doi:10.1097/00005373-198010000-00015

56) Cosma DI, Vasilescu DE, Corbu A, et al. Combined anterolateral, anterior, and anteromedial ankle impingement in an adolescent soccer player: a case report and review of the literature. *Clin J Sport Med*. 2019;29(6):e80-e82. doi:10.1097/JSM.0000000000000576

57) Robinson P, White LM, Salonen DC, Daniels TR, Ogilvie-Harris D. Anterolateral ankle impingement: MR arthrographic assessment of the anterolateral recess. *Radiology*. 2001;221(1):186-190. doi:10.1148/radiol.2211001666

# Post-Traumatic "Floating Fat" in the Extensor Tendon Sheaths of Wrist

Parag Vijaysingh Patil, MD, DNB

## Case Summary

An adult presented with pain and swelling of the right wrist after a fall.

## Imaging Findings

Sagittal reformatted CT of right wrist (Figure 1) demonstrated a comminuted intra-articular fracture of the distal end of the radius (Frykman type VIII). Fat density was noted in the wrist joint space. Axial CT images (Figure 2) demonstrated fat-fluid levels in the extensor pollicis longus (EPL), extensor carpi radialis longus (ECRL), and extensor carpi radialis brevis (ECRB) tendon sheaths. Coronal reformatted CT images (Figure 3) also showed fat densities in EPL, ECRL, and ECRB tendon sheaths.

## Diagnosis

Post-traumatic floating fat in the extensor tendon sheaths of the wrist. Differential diagnosis includes a true synovial lipoma and lipoma arborescens.

**Figure 1.** Sagittal and coronal reformatted CT images of the right wrist with bone reconstruction. Comminuted intra-articular fracture of the distal end of the radius is noted (A), while fat densities are noted in the wrist joint space (B, arrows).

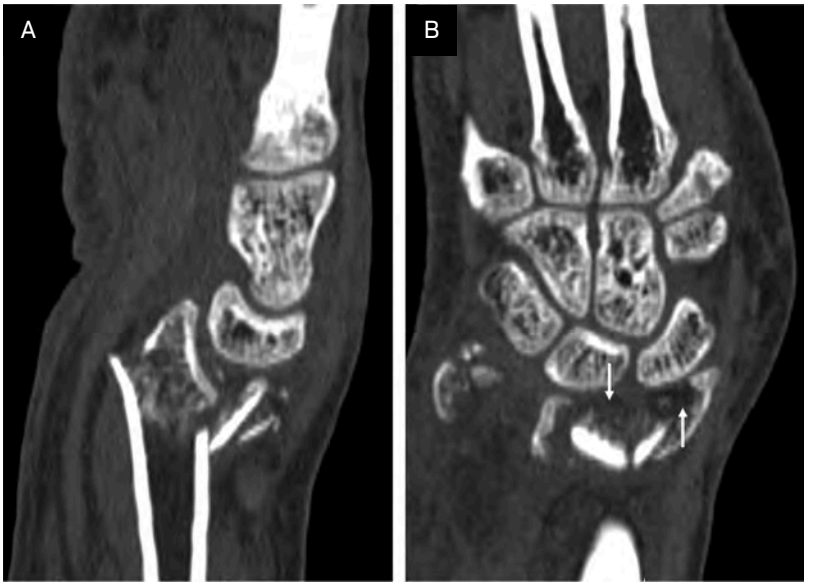


**Figure 2.** Axial CT images of the right wrist with bone reconstruction (A) and soft-tissue reconstruction (B). Fat-fluid levels are noted in the synovial sheaths of extensor pollicis longus (EPL), extensor carpi radialis longus (ECRL), and extensor carpi radialis brevis (ECRB) tendons.

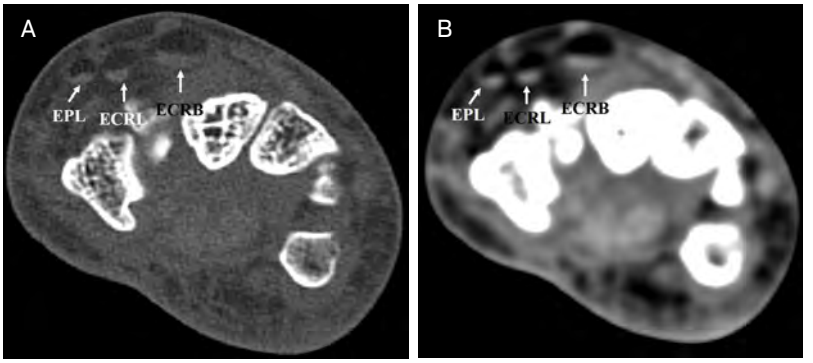


**Affiliation:** Department of Radiodiagnosis, Dr. D. Y. Patil Medical College, Hospital and Research Center, Dr. D. Y. Patil Vidyapeeth, Sant Tukaram Nagar, Pimpri, Pune, Maharashtra, India

**Disclosure:** The authors have no conflicts of interest to disclose. None of the authors received outside funding for the production of this original manuscript and no part of this article has been previously published elsewhere.

Published: July 1, 2025. https://doi.org/10.37549/AR-D-25-0080

**Figure 3.** Coronal reformatted CT images of the right wrist with bone reconstruction (A) and soft-tissue reconstruction (B). Fat densities are noted in the synovial sheaths of extensor pollicis longus (P), extensor carpi radialis longus (L), and extensor carpi radialis brevis (Br) tendons.


## Discussion

Post-traumatic fat-density effusion in the extensor tendon sheath on CT was first reported by Le Corroller et al in 2010.[1] Ali et al observed a similar finding in multiple patients and thought it was an underreported finding.[2] They also suggested that floating fat is a secondary sign of an intra-articular fracture or an occult fracture. In 2017, von Schneider-Egestorf et al retrospectively analyzed MDCT scans of individuals with distal radial intra-articular fractures and found that most of the individuals demonstrated fat-fluid levels in the extensor tendon sheaths.[3] They also found that fracture severity was not related to frequency and severity of tendon sheath involvement.

Bone marrow fat leakage in joints with torn tendon sheaths has been postulated as a cause of fat-density effusion in the joint and tendon sheaths.[3] Tendons of the second extensor compartment (ECRL, ECRB) of the wrist are most often involved, followed by the tendons of the third compartment (EPL). Involvement of both compartments is also common, owing to the existence of a normal foramen between the EPL and ECRB tendon sheaths.[4]

Involvement of the tendon sheaths can be assessed using the Likert scale of semi-quantitative grading from 0 to 2.[3]

## Conclusion

Although floating fat in the extensor tendon sheaths is not uncommon, the condition is an important finding that can indicate the intra-articular extension of a distal radial fracture or an occult fracture and should be recognized.

## References

1) Le Corroller T, Parratte S, Zink J-V, Argenson J-N, Champsaur P. Floating fat in the wrist joint and in the tendon sheaths. *Skeletal Radiol*. 2010;39(9):931-933. doi:10.1007/s00256-010-0929-x

2) Ali S, Huebner S, Groshek F, Schaffer A. The floating fat sign of trauma. *Can Assoc Radiol J*. 2014;65(2):106-112. doi:10.1016/j.carj.2013.02.008

3) von Schneider-Egestorf A, Meyer B, Wacker F, Rosenthal H, von Falck C. Systematic evaluation of concomitant extensor tendon sheath injury in patients with distal intra-articular radial fractures in MDCT using the floating fat sign. *Eur Radiol*. 2017;27(10):4345-4350. doi:10.1007/s00330-017-4787-y

4) Cvitanic OA, Henzie GM, Adham M. Communicating foramen between the tendon sheaths of the extensor carpi radialis brevis and extensor pollicis longus muscles: imaging of cadavers and patients. *AJR Am J Roentgenol*. 2007;189(5):1190-1197. doi:10.2214/AJR.07.2281

*"I wish I could play little league now. I'd be way better than before."*

*—Mitch Hedberg*

**Dr Phillips** is a professor of Radiology, director of Head and Neck Imaging, at Weill Cornell Medical College, New York Presbyterian Hospital, New York, New York. He is a member of the *Applied Radiology* Editorial Advisory Board.

# Weird Cases

C. Douglas Phillips, MD, FACR

I believe Mitch Hedberg said more truisms in his short life than 99% of humans on this planet. This is a gem and goes right to what I want to talk about. Experience. Please notice I didn't call it wisdom; I'm not talking about a deep philosophical approach to getting old (which I am) but making a more directed observation. Seeing things over and over is a great way to learn. I write this at the end of another academic year; another group of residents off to become fellows or staff somewhere. Another group of fellows off to become worker bees somewhere (or do another fellowship). This is a time of some modest reflection.

Here's the gist of it: early in your career (and for the sake of this piece, let's pretend that you've completed training and you are the ATTEND-ING now, in private practice, an academic shop, whatever). Okay, so you're working. You're sitting there, pulling up cases and making with the words. And you're killing it. You are *awesome*. And then you open a case, and…you have absolutely no idea what you're looking at. You quietly hyperventilate and sip some more coffee and look again, except nothing changes. It still looks like whatever, and you have no earthly idea what it is.

Early in your career, I'll tell you exactly what goes through your head—you have no clue if this is truly a weird case, or you are just a moron. It can shake you in ways you didn't imagine could happen. So, you page Dr. Google, or open a teaching aid you know and love, or maybe grab a partner/colleague—one with gray hairs and a few years. And, usually, they have something for you. And you recover until the next one. After a few years, you might see another case like this, but the next time you've got some muscle memory, and you remember! Well, hopefully. Experience is like speed. You can't teach it.

Experience matters in another important way. Perhaps more importantly than just having seen those oddities of life, you now know what to ignore. I like to have people point out to me that I didn't describe some *meaningless, incidental thing*. I choose to ignore those; that way I don't scare patients and waste my time. Feel free to describe and measure those pineal calcifications or measure those normal lymph nodes; have at it.

So, I guess I won't be able to go back and play little league ball again (although I would absolutely kick ass this time), but I do have some experience, and I know a few things. I won't waste too much time on incidental nothings, and I will likely know one or two of those weird cases, or at least be able to give you a great differential. Maybe I'll join you in that quiet hyperventilation and search for more caffeine.

Keep doing that good work. Mahalo.